DOKUZ EYLUL UNIVERSITY
GRADUATE SCHOOL OF NATURAL AND APPLIED SCIENCES

PRODUCTION OF HAP FILMS ON 316L SS AND THEIR CHEMICAL AND MORPHOLOGICAL CHARACTERISTICS

by
Hakan TANSUĞ

June, 2008
İZMİR

PRODUCTION OF HAP FILMS ON 316L SS AND THEIR CHEMICAL AND MORPHOLOGICAL CHARACTERISTICS

A Thesis Submitted to the
Graduate School of Natural and Applied Sciences of Dokuz Eylül University
In Partial Fulfillment of the Requirements for the Degree of Master of Science
in Metallurgy and Materials Engineering, Metallurgy and Materials Program

by
Hakan TANSUĞ

June, 2008
İZMİR

M.Sc. THESIS EXAMINATION RESULT FORM

We have read the thesis entitled **"PRODUCTION OF HAP FILMS ON 316L SS AND THEIR CHEMICAL AND MORPHOLOGICAL CHARACTERISTICS"** completed by **HAKAN TANSUĞ** under supervision of **ASSIST. PROF. DR. UĞUR MALAYOĞLU** and we certify that in our opinion it is fully adequate, in scope and in quality, as a thesis for the degree of Master of Science.

……..…….

Assist. Prof. Dr. Uğur MALAYOĞLU

Supervisor

…….. ……

Prof. Dr. Ahmet ÇAKIR — Assoc. Prof. Dr. Hasan YILDIZ

(Jury Member) (Jury Member)

Prof. Dr. Cahit HELVACI

Director

Graduate School of Natural and Applied Sciences

ACKNOWLEDGMENTS

I cordially would like to express my thanks to my supervisor, Assist. Prof. Uğur Dr. MALAYOĞLU for his guidance, interest and support.

I would like to thank to Technical and Scientific Council of Turkey, TUBITAK for financial support provided to fund project number 106M316. Thanks are also extended to DEU University for their support in encouraging scientific researches in general.

I would like to present my gratitude to Prof. Dr. Ahmet ÇAKIR who is headman of TUBITAK project for his efforts to improve my theoretical background.

I'd like to extend my appreciation to Assist. Prof. Dr. Aylin Ziylan ALBAYRAK for her assistance and advices.

I also would like to thank my colleagues, M.Sc students, Güler Ungan and Pınar Köymen, for their cooperation, friendship and patience.

Finally, I would like to thank my all family for their support and patience.

Hakan TANSUĞ

PRODUCTION OF HAP FILMS ON 316L SS AND THEIR CHEMICAL AND MORPHOLOGICAL CHARACTERICS

ABSTRACT

The hydroxyapatite (HA) coatings have long been widely used on implant materials as thin films. 316L stainless steel (SS) was used as metallic biomaterial because of their superior strength, biocompatibility, durability and resistance to corrosion in physiological environment. The main objective of this thesis was to form HA coatings on medical grade 316L SS in an electrolyte containing Ca^{2+} and $H_2PO_4^-$ ions by using an galvanostatic electrochemical deposition technique and investigate the chemical composition and morphology of these coatings. The phases of depositions were characterized by X-Ray diffraction (XRD) and Fourier transform infra-red spectroscopy (FTIR). Morphology of the coatings was investigated by scanning electron microscope (SEM). Ca/P atomic and weight and ratios calculated by energy dispersion spectroscopy (EDS) analysis and results compared with the quantitative analysis of crystalline components in the XRD patterns. The average crystal size of HA coatings was calculated by the Scherrer's equation. It's concluded that galvanostatic electrochemical deposition is a useful technique to deposit HA coatings on 316L SS. The results showed that deposition parameters like current density, total amount of charge, electrolyte concentration and process temperature were determiner for which calcium phosphate phase will be deposited and they mainly affect the morphological structure of the coatings.

Keywords: Hydroxyapatite, galvanostatic electrochemical deposition, 316L

316L PÇ ÜZERİNDE HAP FİLMLERİN ÜRETİMİ VE KİMYASAL VE MORFOLOJİK ÖZELLİKLERİ

ÖZ

Hidroksiapatit (HA) kaplamalar uzun bir süredir implant malzemeler üzerinde ince film olarak yaygın bir şekilde kullanılmaktadır. 316L paslanmaz çeliği (PÇ) üstün mukavemeti, biyouyumluluğu, dayanıklılığı ve fiziksel ortamlardaki korozyona karşı olan direnci nedeniyle metalik biyomalzeme olarak kullanılmaktadır. Bu tezin temel amacı galvanostatik elektrokimyasal çöktürme tekniği kullanılarak Ca^{2+} ve $H_2PO_4^-$ içeren elektrolitlerden HA kaplamaların üretimi ve kaplamaların kimyasal kompozisyon ve morfolojik yapılarının incelenmesidir. Kaplamaların faz analizi X-ışınları difraktometrisi (XRD) ve FTIR ile karakterize edilmiştir. Kaplamaların morfolojileri taramalı elektron mikroskopu ile incelenmiştir. Ca/P atomic ve ağırlıkça oranları enerji dağılım spektrometresi (EDS) ile hesaplanmıştır ve sonuçlar XRD paternlerindeki kristalik bileşenlerin kantitatif analizi ile karşılaştırılmıştır. HA kaplamaların ortalama Kristal boyutu Scherrer eşitliğine göre hesaplanmıştır. Galvanostatik elektrokimyasal çöktürme tekniğinin 316L PÇ üzerinde HA kaplamaların çöktürülebilmesi için uygun bir yöntem olduğu sonucuna varılmıştır. Akım yoğunluğu, toplam yük miktarı, elektrolit konsantrasyonu ve işlem sıcaklığı gibi çöktürme parametrelerinin hangi kalsiyum fosfat fazının oluşacağında belirleyici olduğu ve bu parametrelerin kapmaların morfolojik yapısını temel olarak etkiledikleri bulunmuştur.

Anahtar sözcükler: Hidroksiapatit, galvanostatik elektrokimyasal çöktürme, 316L

CONTENTS

Page

CHAPTER ONE
INTRODUCTION

Biomaterials have received much interest and intensive research during the last few decades, due to their obvious use as replacements of various body parts or even organs. Their use and the improvement of their reliability and life span would undoubtedly improve the quality of human life in more than one aspect.

Austenitic stainless steels are popular for implant applications because they are relatively inexpensive and can be formed with common techniques by which mechanical properties can be controlled over a wide range for optimal strength and ductility. Austenitic stainless steels are not sufficiently corrosion resistant for long-term use as an implant material. They find use as bone screws, bone plates, intramedullary nails and rods, and other temporary fixation devices (Davis, 2004). The most widely used austenitic stainless for medical and dental applications is AISI 316L stainless steel.

The major inorganic constituent of bones and teeth is a calcium phosphate phase with a composition similar to that of synthetic hydroxyapatite (HA; $Ca_5(PO_4)_3OH$). Coating biologically inert metallic implants with biologically active materials, like HA, attempt to accelerate bone formation on initial stages of osseointegration, thus improving implant fixation (Vidigal et al., 1999). HA coatings also reduced metal ions release by acting as a pyscial barrier (Lazic et al., 2001).

The HA coating, however, gives rise to problems including composition and structure control, and tightly bonding to the substrate (Kangasniemi et al., 1994; Wang et al., 1995). To overcome to this problems different coating techniques have been developed .

The most widely applied coating procedure today is the plasma spray coating method. HA subjected to the extreme high temperatures of a plasma flame results in

structural modifications of the applied ceramic coating and is restricted to line of sight application (Dasarathy et al., 1996).

Electrochemical deposition methods that may eliminate the problems associated with the high temperature coating process of plasma spray have received much attention in the area of bioactive surface modification. The electrochemical technique is a low-temperature process using aqueous electrolytes which is prepared by dissolving reagent-grade $Ca(NO_3)_2 \cdot 4H_2O$ and $NH_4H_2PO_4$ in distilled water. It has been shown that the CaP coatings prepared by this method are uniform and adherent (Shirkhanzadeh, 1995). It has also been seen that this process allows porous surfaces to be coated uniformly without clogging the pores. Studies have been shown that morphology and microstructure can be regulated by controlling the composition of the electrolyte, the electrolyte temperature, the current density, the current loading time, and the composition of the substrate metal (Ban & Maruna, 1998).

Primary objectives of this thesis were the following:

1. To form HA coatings on medical grade 316L Stainless Steel by using a galvanostatic electrochemical deposition technique which is applying at constant current.

2. To study the effects of electrochemical deposition parameters (applied current density, total amount of charge, electrolyte concentration, deposition temperature etc.) on the crystal structure and chemical composition of the CaP coatings.

3. To develop efficiency alkaline treatment for converting Brushite to Hydroxyapatite and investigate the morphological changes and phase transformations after the treatment.

CHAPTER TWO
TYPES OF MATERIALS USED IN MEDICAL APPLICATIONS

2.1 Introduction

Metals have been successfully used as biomaterials for many years. Materials and systems for biological use have been synthesized and fabricated in a wide variety of shapes and forms, including composites and coated systems. Some of the new materials and technologies have been developed especially for biological uses, while others have been borrowed from such unexpected areas as space technology.

Relatively few metals in industrial use are biocompatible and capable of long-term success as an implant in the body. In developing a biomedical alloy, non-toxic elements must be selected as alloying elements. The biocompatibility of pure metals and some metallic biomedical alloys are compared in Fig.2.1. For structural applications in the body (e.g., implants for hip, knee, ankle, shoulder, wrist, finger, or toe joints), the principal metals are stainless steels, cobalt-base alloys, and titanium-base alloys. These metals are popular primarily because of their ability to bear significant loads, withstand fatigue loading, and undergo plastic deformation prior to failure. Other metals and alloys employed in implantable devices include commercially pure titanium (CP-Ti), shape memory alloys (al1oys based on the nickel-titanium binary system), zirconium alloys, tantalum (and, to a lesser extent, niobium), and precious metals and al1oys (Niinomi, 1999).

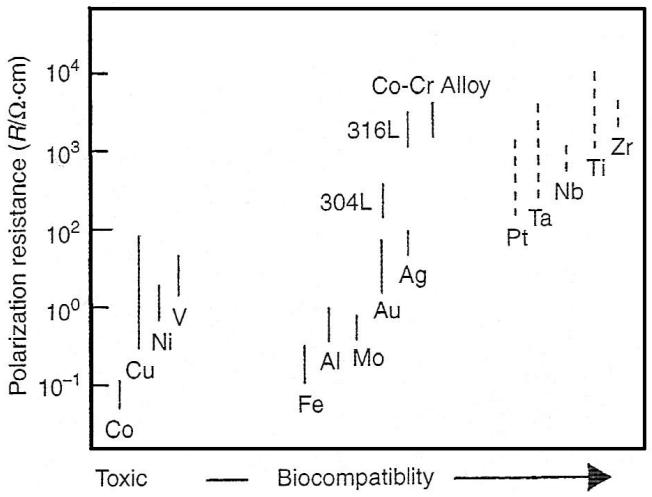

Figure 2.1 The relationship between polarization resistance and biocompatibility of pure metals, cobalt-chromium alloy, and stainless steels (Niinomi, 1999).

Alloys used in articulating prosthesis applications are often used in conjunction with other biomaterials, such as ultrahigh molecular weight polyethylene (UHMWPE), polyoxymethylene (Delrin-150, E.I. DuPont de Nemours & Co.), or aluminium oxide ceramics. A typical hip prosthesis consists of the stern, a ball, and a socket with a metallic backing.

The chemistry and manufacturing processes for metallic biomaterials are not necessarily unique to the biomedical device industry. Control of undesired elements is an important aspect of the successful application of metal1ic biomaterials. The principal requirement for each alloy is that it be corrosion resistant when inserted in the body and that it have optimal mechanical properties.

Stainless steels and cobalt-chromium alloys depend for their general corrosion resistance on the presence of chromium and its ability to render the alloys passive. Additions of other alloy elements enhance resistance to nonuniform types of corrosion (e.g., pitting). Titanium and titanium alloys develop passivity without chromium. Surface passivity is the most important criteria, but surface finish also can affect performance. Highly polished surfaces perform better in terms of corrosion and wear (Ratner et al., 1996).

2.2 Classes of Materials Used In Medicine

2.2.1 Steps in the Fabrication of Implants

Understanding the structure and properties of metallic implant materials requires an appreciation of the metallurgical significance of the material's processing history. Since each metallic device differs in the details of its manufacture "generic" processing steps are presented in Fig. 2.2.

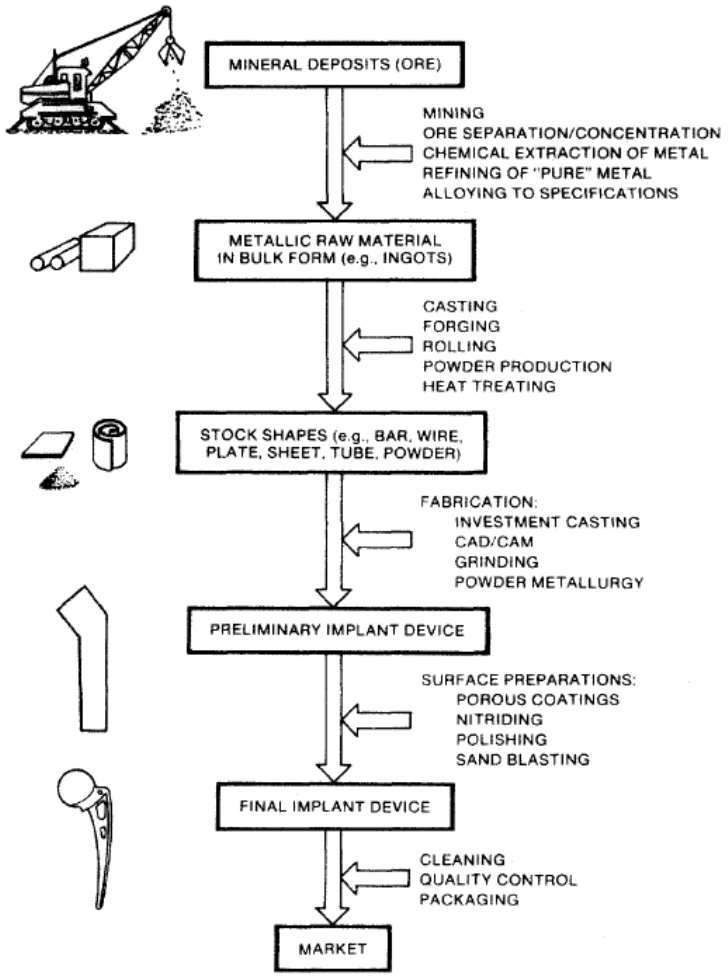

Figure 2.2 General processing history of a typical metallic implant device, in this case a hip implant (Ratner et al., 1996).

2.2.1.1 Metal-Containing Ore to Raw Metal Product

With the exception of the noble metals (which do not represent a major fraction of implant metals), metals exist in the Earth's crust in mineral form and are chemically combined with other elements, as in the case of metal oxides. These mineral deposits (ore) must be located and mined, and then separated and enriched to provide ore suitable for further processing into pure metal.

In the case of multi component metallic implant alloys, the raw metal product will have to be processed further. Processing steps include remelting, the addition of alloying elements, and solidification to produce an alloy that meets certain chemical specifications. For example, to make ASTM (American Society for Testing and Materials) F138 316L stainless steel, iron is alloyed with specific amounts of carbon, silicon, nickel, and chromium. To make ASTM F75 or F90 alloy, cobalt is alloyed with specific amounts of chromium, molybdenum, carbon, nickel, and other elements (Ratner et al., 1996).

2.2.1.2 Raw Metal Product to Stock Metal Shapes

A manufacturer further processes the bulk raw metal product (metal or alloy) into "stock" shapes, such as bars, wire, sheet, rods, plates, tubes, and powders. These shapes are then sold to specialty companies (e.g., implant manufacturers) who need stock metal that is closer to the actual final form of the implant.

Bulk forms are turned into stock shapes by a variety of processes, including remelting and continuous casting, hot rolling forging, and cold drawing through dies. Depending on the metal, there may also be heat-treating steps (heating and cooling cycles) designed to facilitate further working or shaping of the stock, relieve the effects of prior plastic deformation (e.g. annealing), or produce a specific microstructure and properties in the stock material. Because of the chemical reactivity of some metals at elevated temperatures, high-temperature processes may require vacuum conditions or inert atmospheres to prevent unwanted uptake of

oxygen by the metal. For instance in the production of fine powders of ASTM F75 Co-Cr-Mo alloy, molten metal is ejected through a small nozzle to produce a fine spray of atomized droplets that solidify while cooling in an inert argon atmosphere (Ratner et al., 1996). For metallic implant materials in general, stock shapes are chemically and metallurgically tested to ensure that the chemical composition and microstructure of the metal meet industry standards for surgical implants (ASTM Standards).

2.2.1.3 Stock Metal Shapes to Preliminary and Final Metal Devices

Typically, an implant manufacturer will buy stock material and then fabricate it into preliminary and final forms. Specific steps depend on a number of factors, including the final geometry of the implant, the forming and machining properties of the metal, the costs of alternative fabrication methods, and the company doing the fabrication. Fabrication methods include investment casting (the "lost wax" process), conventional and computer-based machining (CAD/CAM), forging, powder metallurgical processes (hot isostatic pressing, or HIP), and a range of grinding and polishing steps. A variety of fabrication methods are required because not all implant alloys can be feasibly or economically made in the same way. For instance, cobalt-based alloys are extremely difficult to machine into the complicated shapes of some implants and are therefore frequently shaped into implant forms by investment casting or powder metallurgy. On the other hand titanium is relatively difficult to cast and therefore is frequently machined even though it is not generally considered to be an easily machinable metal (Pillar & Weatherly, 1984).

Another aspect of fabrication, which is actually an end-product surface treatment, involves the application of macro or micro porous coatings on implants. This has become popular in recent years as a means to facilitate fixation of implants in bone. The porous coatings can take various forms and require different fabrication technologies. In turn, this part of the processing history will contribute to metallurgical properties of the final implant device. In the case of alloy beads or "fiber metal" coatings, the manufacturer will apply the coating material over specific

regions of the implant surface (e.g., on the proximal portion of the femoral stem), and then attach the coating to the substrate by a process such as sintering. Generally, sintering involves heating the construct to about one-half or more of the alloy's melting temperature to enable diffusive mechanisms to form necks that join the beads to one another and to the implant's surface. An alternative surface treatment to sintering is plasma or flame spraying a metal onto an implant's surface. A hot, high velocity gas plasma is charged with a metallic powder and directed at appropriate regions of an implant surface. The powder particles fully or partially melt and then fall onto the substrate surface, where they solidify rapidly to form a rough coating. Other surface treatments are also available, including ion implantation (to produce better surface properties) and nitriding. In nitriding, a high-energy beam of nitrogen ions is directed at the implant under vacuum. Nitrogen atoms penetrate the surface and come to rest at sites in the substrate. Depending on the alloy, this process can produce enhanced properties. These treatments are commonly used to increase surface hardness and wear properties. Finally, metallic implant devices usually undergo a ser of finishing steps. These vary with the metal and manufacturer, but typically include chemical cleaning and passivation (i.e., rendering the metal inactive) in appropriate acid, or electrolytically controlled treatments to remove machining chips or impurities that may have become embedded in the implant's surface. As a rule, these steps are conducted according to good manufacturing practice (GMP) and ASTM specifications for cleaning and finishing implants. In addition, these steps can be extremely important to the overall biological performance of the implant (Kasemo & Lausmaa, 1988).

2.2.2 Stainless Steels

Stainless steels are iron-base alloys that contain a minimum of 10.5% Cr, the amount needed to prevent the formation of rust in unpolluted atmospheres (hence the designation stainless). Few stainless steels contain more than 30% Cr or less than 50% Fe. They achieve their stainless characteristics through the formation of an invisible and adherent chromium-rich oxide surface film (~2 nm thick). This oxide forms and heals itself in the presence of oxygen (Davis, 2004).

Increasing the chromium content beyond the minimum of 10.5% confers still greater corrosion resistance. Further improvement in corrosion resistance and a wide range of properties may be achieved by the addition of nickel. The addition of other alloying elements may be used to enhance resistance to specific corrosion mechanisms or to deve1op desired mechanical and physical properties. For example, molybdenum further increases resistance to pitting corrosion, while nitrogen increases mechanical strength as well as enhances resistance to pitting. Carbon is normally present in amounts ranging from less than 0.03% to over 1.0% in certain martensitic grades (Davis, 2004).

Approximately 1% of the total tonnage of stainless steels is used for biomedical applications. Most nonimplant medical devices (e.g., surgical and dental instruments) are manufactured from commercial-grade stainless steels. These stainless steels adequately meet clinical requirements where contact with human tissue is transient.

Stainless steels used for implants must be suitable for close and prolonged contact with human tissue (i.e., warm, saline conditions). Specific requirements for resistance to pitting and crevice corrosion and the quantity and size of nonmetallic incIusions apply to implant-grade stainless steels. Hence, special production routes such as vacuum melting (VM), vacuum arc remelting (VAR), or electroslag refining (ESR) are required to produce implant steels (Pillar & Weatherly, 1984).

While several types of stainless steels are available for implant use (Table 2.1), in practise is most common is 316L (ASTM F138, F139), grade 2. This steel has less than 0.030% (wt. %) carbon in order to reduce the possibility of in vivo corrosion. The “L” in the designation 316L denotes its low carbon content. The 316L alloy is predominantly iron (60-65%) alloyed with major amounts of chromium (17-19%) and nickel (12-14%), plus minor amounts of nitrogen, manganese, molybdenum, phosphorous, silicon and sulphur (Ratner et al., 1996).

Table 2.1 Chemical composition of stainless steels used for implants (Ratner et al., 1996).

Material	ASTM designation	Common/trade names	Composition (wt %)	Notes
Stainless steel	**F55 (bar, wire)**	**AISI 316LVM**	60-65 Fe	F55, F56 specify 0.03 max for P, S.
	F56 (sheet, strip)	**316L**	17.00-19.00 Cr	F138, F139 specify 0.025 max for P and 0.010 max for S.
	F138 (bar, wire)	**316L**	12.00-14.00 Ni	LVM = Low vacuum melt
	F139 (sheet, strip)	**316L**	2.00-3.00 Mo	
			Max 2.0 Mn	
			Max 0.5 Cu	
			Max 0.03 C	
			Max 0.1 N	
			Max 0.025 P	
			Max 0.75 Si	
			Max 0.01 S	
Stainless Steel	**F745**	**Cast stainless steel 316L**	60-69 Fe	
			17.00-19.00 Cr	
			11.00-14.00 Ni	
			2.00-3.00 Mo	
			Max 0.06 C	
			Max 2.0 Mn	
			Max 0.045 P	
			Max 1.00 Si	
			Max 0.030 S	

2.2.3 Cobalt Based Alloys

Cobalt-base alloys were first used in the 1930s. The Co-Cr-Mo alloy Vitallium was used as a cast dental alloy and then adopted to orthopedic applications starting in the 1940s (Davis, 2004). The corrosion of cobalt-chromium alloys is more than an order of magnitude greater than that of stainless steels, and they possess high mechanical property capability. Although cobalt alloys were first used as cast components, wrought alloys later came into use. Although a number of specifications exist for cobalt-base alloys, the four main alloys used are:

- ASTM F75, Co-28Cr-6Mo casting alloy
- ASTM F90, Co-20Cr-15W-10Ni wrought alloy
- ASTM F799, Co-28Cr-6Mo thermomechanically processed alloy with a composition nearly identical to ASTM F75 casting alloy

- ASTM F562, Co-35Ni-20Cr-10Mo wrought alloy

Compositions for these and other alloys covered by ASTM specifications are listed in Table 2.2.

Table 2.2 Chemical compositions of cobalt-base alloys used for surgical implants (Davis, 2004).

		Composition(s), wt %										
ASTM designation	**UNS No.**	**Cr**	**Mo**	**Ni**	**Fe**	**C**	**Si**	**Mn**	**W**	**P**	**S**	**Others**
F75	**R30075**	27-30	5-7	1.0	0.75	0.35	1.0	1.0	0.2	0.02	0.01	0.25 N; 0.30 Al; 0.01 B
F90	**R30605**	19-21	…	9.00 - 11.0	3.00	0.05-0.15	0.4	1.0-2.0	14-16	0.04	0.03	…
F562	**R30035**	19-21	9-10.5	33-37	1.00	0.025	0.15	0.15	…	0.015	0.010	1.0 Ti
F563	**R30563**	18-22	3-4	15-25	4.00 - 6.00	0.05	0.50	1.00	3.0 - 4.0	…	0.010	0.50-3.60 Ti
F799	**R31537**	26-30	5-7	1.00	0.75	0.35	1.00	1.00	…	…	…	0.25 N
F1058 grade 1	**R30003**	19-21	6-8	14-16	Bal (b)	0.15	1.20	1.5-2.5	…	0.015	0.015	0.10 Be; 39-41 Co
F1058 grade 2	**R30008**	18.5 - 21.5	6.5-7.5	15-18	Bal (b)	0.15	1.20	1.20	…	0.015	0.015	0.001Be ; 39-42 Co
(a) Single values are maximum values unless otherwise indicated. (b) The iron content is approximately equal to the difference between 100% and the sum percentage of the other specified elements. ASTM F1058 grade 1 contains between 39.0 and 41.0 wt% Co; ASTM F1058 grade 2 contains between 39.0 and 42.0 wt% Co												

Strengthening in cobalt alloys is produced by solid-solution elements and the presenee of carbides. In wrought alloys where working is possible, cold work enhanees strength. In order to produee wrought coba1t-chromium alloys, carbon must be reduced compared to the level in cast alloys (0.05% versus approximately 0.25% or higher). Low earbon contents mean that less strengthening is produced by carbides. To enhance fabricability, chromium contents generally are reduced and nickel added. Wrought alloys can be hot worked, and some can be cold drawn. Yield strengths vary with grain size and the degree of cold work imparted from the wrought fabrication process (Ratner et al., 1996).

Alloys produced for structural applications such as hip prostheses can be forged if optimal properties are desired. The forging process results in maximum strength and

toughness for cobalt-chromium alloys but may not produce uniform grain sizes. Data have been reported on forging of a modified F75 composition wherein finer grain size occurred in the distal end (tip of the femoral stern, farthest from the ball) than in the proximal end (Table 2.3). Strength (fatigue, yield) was correspondingly better in specimens taken from the distal end (Donachie, 1998).

Table 2.3 Effect of forging on Vitallium alloy (Co-28Cr-6Mo) mechanical properties (Donachie, 1998).

	Tensile strength		**0.2% yield strength**			**Fatigue strength (10^6 cycles implied, R=-1)**	
Material condition	MPa	ksi	MPa	ksi	Elongation, %	MPa	ksi
Forged							
Proximal stem	1406.6	204.0	889.5	129.0	28.3	792.9	115.0
Distal stem	1506.6	218.5	1029.4	149.3	27.5	827.4-965.3	120-140
Cast(typical)	790	115	520	75	15	310	45

Cobalt-chromium alloys are difficult to machine. Closed-die forging can minimize machining requirements, but wrought processedcomponents stilI may require more machining than cast components. Consequently, investment casting often is used to produce cobalt chromium implants at the lowest cost. The grain size of cast components is invariably greater than that of comparable wrought components, so strength properties of castings do not approach those of wrought cobalt-chromium alloys. Porosity can be a problem in castings but can be controlled by improved mold design and by application of hot isostatic pressing (HIP) in postcast treatment of vacuum investment-cast alloys. Powder metallurgy has been used to make some cobalt-chromium components. Hot isostatic pressing of powder is claimed to result in very fine grains and exceptional properties, but costs may be higher (Compte, 1984).

The preferred method of producing cobaltbase alloy implants will be a function of the trade-offbetween cost and properties. Where the properties of castings are sufficient, castings will dominate. When maximum strength is required, hot pressing and/or forging will role. Table 2.4 shows that forged, cold-worked, and HIPed wrought cobalt alloys have substantial mechanical property advantages over the cast alloy (Brunski, 1996).

Table 2.4 Typical properties of cast and wrought cobalt-base alloys (Brunski, 1996).

		Young's modulus		Yield strength		Tensile strength		Fatigue endurance limit (at 10^7 cycles, R=-1)	
ASTM designation	**Condition**	GPa	10^6 psi	MPa	ksi	MPa	ksi	MPa	ksi
F 75	**As-cast/ annealed**	210	30	448-517	65-75	655-889	95-129	207-310	30-45
	P/M HIP(a)	253	37	841	122	1277	185	725-950	105-138
F 799	**Hot forged**	210	30	896-1200	130-174	1399-1586	203-230	600-896	87-130
F 90	**Annealed**	210	30	448-648	65-94	951-1220	138-177	Not available	
	44% cold worked	210	30	1606	233	1896	275	586	85
F 562	**Hot forged**	232	34	965-1000	140-145	1206	175	500	73
	Cold worked, aged	232	34	1500	218	1795	260	689-783(b)	100-115(b)
(a) P/M, powder metallurgy; HIP, hot isostatic pressing. (b) Axial tension, R=0.05, 30Hz									

2.2.4 Titanium and Titanium-Base Alloys

Titanium is a low-density element (approximately 60% of the density of iron) that can be highly strengthened by alloying and deformation processing. Titanium and its alloys used for implant devices have been designed to have excellent biocompatibility, with little or no reaction with tissue surrounding the implant. Titanium derives it corrosion resistance from the stable oxide film that forms on its surface, which can reform at body temperatures and in physiological f1uids if damaged. Increased use of titanium alloys as biomaterials is occurring due to their lower modulus (see, for example, Table 2.5), superior biocompatibility, and enhanced corrosion resistance when compared to more conventional stainless steels and cobaltbase alloys. These attractive properties were a driving force for the early introduction of commercially pure titanium (CP-Ti) and α+β (Ti-6Al-4V) alloys as well as for the more recent development of new titanium alloy compositions and orthopedic metastable β alloys (Donachie, 1998).

Table 2.5 Comparison of mechanical properties of metallic implant materials with those of cortical bone (Donachie, 1998).

Material	Young's modulus		Ultimate tensile strentgh		Fracture thougness	
	GPa	10^6 psi	GPa	10^6 psi	MPa/$m^{½}$	ksi/$in.^{½}$
Cobalt-chromium alloys	230	35	900-1540	130-225	~100	~90
Austentic stainless steels	200	30	540-1000	80-145	~100	~90
Ti-6Al-4V	106	15	900	130	~80	~70
Cortical bone	7-30	1-4	50-150	7-20	2-12	2-11

As shown in Table 2.6, there are four ASTM standardized α-β alloys currently used for medical devices. Ti-6AI-4V and Ti-6AI-4V ELI are the most commonly employed alloys. They are widely used for total joint replacement arthroplasty.

Table 2.6 ASTM specifications, nominal compositions, and UNS designations for titanium and titanium alloys used for biomedical applications (Davis, 2004).

ASTM specification	Alloy	UNS No.
Alpha microstructures		
F67	CP-Ti grade 1	R50250
	CP-Ti grade 2	R50400
	CP-Ti grade 3	R50550
	CP-Ti grade 4	R50700
Alpha-beta microstructures		
F136	Ti-6Al-4V ELI	R56401
F1472	Ti-6Al-4V	R56400
F1295	Ti-6Al-7Nb	R56700
F2146	Ti-3Al-2.5V	R56320
Beta microstructures		
F1713	Ti-13Nb-13Zr	…
F1813	Ti-12Mo-6Zr-2Fe	R58120
F2066	Ti-15Mo	R58150

CP titanium (ASTM F67) and extra-low interstitial (ELI) Ti-6Al-4V alloy (ASTM F136) are the two most common titanium-based implant biomaterials. The F67 CP Ti is 98.9-99.6% titanium (Table 2.7).

Table 2.7 Chemical Compositions of Ti-Based Alloys for Implants (Ratner et al., 1996).

Material	ASTM designation	Common/trade names	Composition (wt %)	Notes
Pure Ti	**F67**	**CP Ti**	Balance Ti	CP Ti comes in four grades according to oxygen content only grade 4 is listed
			max 0.10 C	
			max 0.5 Fe	
			max 0.0125-0.015 H	
			max 0.05 N	
			max 0.40 O	
Ti-6Al-4V	**F136**	**Ti-6Al-4V**	88.3-90.8 Ti	
			5.5-6.5 Al	
			3.5-4.5 V	
			max 0.08 C	
			0.0125 H	
			max 0.25 Fe	
			max 0.05 N	
			max 0.13 O	

Oxygen content of CP Ti affects its yield and fatigue strength significantly. For example, at 0.18% oxygen (grade 1), the yield strength is about 170 MPa, while at 0.40% (grade 4), the yield strength increases to about 485 MPa. Similarly, at 0.085 wt.% oxygen (slightly purer than grade 1) the fatigue limit (10^7 cycles) is about 88.2 MPa, while at 0.27 wt.% oxygen (slightly purer than grade 2) the fatigue limit (10^7 cycles) is about 216 MPa (Beveers & Robinson, 1969).

With Ti-6Al-4V ELI alloy, the individual Ti-Al and Ti-V the phase diagrams suggest the effects of the alloying additions in the ternary alloy. Al is an alpha (HCP) phase stabilizer while V is a beta (BCC) phase stabilizer. The 6Al-4V alloy is used for implants is an alpha-beta alloy, properties which vary with prior treatments.

2.2.5 Polymers

Polymers are considered for implant applications in various forms such as fibres, textiles, rods and viscous liquids. Recently, polymers have been introduced for hip socket replacement in orthopaedic implant applications due to its close resemblance to natural polymeric tissue components. However, polymers undergo degradation in

the body environment due to biochemical and mechanical factors. This results in ionic attack and formation of hydroxyl ions and dissolved oxygen, leading to tissue irritation and decrease in mechanical properties. Many types of polymers are used for biomedical purposes Figure 2.3 illustrates the variety of clinical applications for polymeric biomaterials.

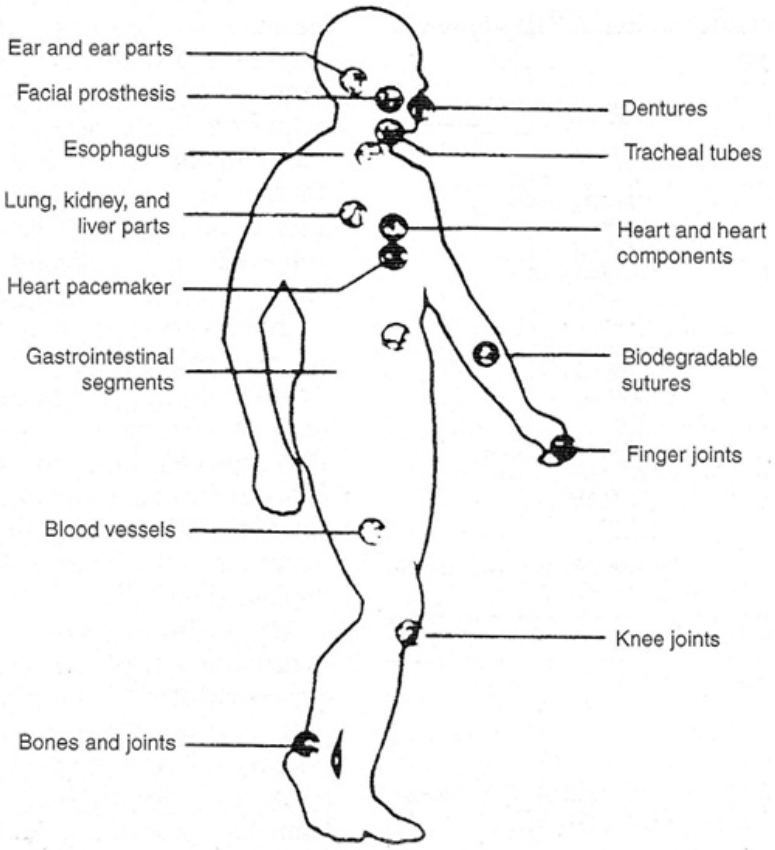

Ear and ear parts: acrylic, polyethylene, silicone, poly(vinyl chloride) (PVC)
Dentures: acrylic, ultrahigh molecular weight polyethylene (UHMWPE), epoxy
Facial proshthesis: acrylic, PVC, polyurethane (PVC)
Tracheal tubes: acrylic, silicone, nylon
Heart and heart components: polyester, silicone, PVC
Heart pacemaker: polyethylene, acetal
Lung, kidney, and liver parts: polyester, polyaldehyde, PVC
Eshophagus segments: polyethylene, polypropylene (PP), PVC
Blood vessels: PVC, polyester
Biodegradable sutures: PUR
Gastrointestinal segments: silicones, PVC, nylon
Finger joints: silicone, UHMWPE
Bones and joints: acrylic, nylon, silicon, PUR, PP, UHMWPE
Knee joints: polyethylene

Figure 2.3 Common clinical applications and types of polymers used in medicine (Ratner et al., 1996).

2.2.6 Ceramics

Ceramics are inorganic compounds that can be classified into five categories of biomaterials by their macroscopic surface characteristics or by their chemical stability in the body environment. They are carbon, alumina, zirconia, bioactive glass (glass ceramics) and calcium phosphate. The limitations of ceramic materials are their low tensile strength and fracture toughness. Their use in bulk form is therefore limited to functions in which only compressive loads are applied. Results of ex-vivo push-out tests indicate that the ceramic/metal bond fails before the integration of the ceramic/tissue bond because of the weak link in the system (Hench 1982). Thus, there is reason for concern about the weak ceramic/metal bond and the integrity of this interface over a lengthy service-life under functional loading.

2.2.6.1 Calcium Phosphate Ceramics

Calcium-phosphate-based bioceramics have been in use in medicine and densitry for nearly thirty years. Applications include dental implants, periodontal treatment, alveolar ridge augmentation, orthopedics, maxillofacial surgery, and otolaryngology (Davis, 2004). Different phases of calcium phosphate ceramics are used depending on whether a resorbable or bioactive material is desired.

The stable phases of calcium phosphate ceramics depend considerably on temperature and the presence of water, either during processing or in the use environment. At body temperature, only two calcium phosphates are stable in contact with aqueous media, such as body fluids; at pH < 4.2, the stable phase is $CaHPO_4 \cdot 2H_20$ (dicalciumphosphate or brushite), while at pH ≥ 4.2, the stable phase is $Ca_{10}(PO_4)_6(OH)_2$ (hydroxylapatite,HA). At higher temperatures, other phases, such as $Ca_3(PO_4)_2$ (β-tricalciumphosphate, C_3P, or TCP) and $Ca_4P_2O_9$ (tetracalcium phosphate, C_4P),are present. The unhydrated high-temperature calcium phosphate phases interact with water, or body fiuids, at 37 ºC to form HA. The HA forms on exposed surfaces of TCP by the following reaction:

$$4Ca_3(PO_4)_2 + 2H_2O = Ca_{10}(PO_4)_6(OH) + 2Ca^{2+} + 2H_2PO_4^{2-} \quad (2.1)$$

Thus, the solubility of a TCP surface approaches the solubility of HA and decreases the pH of the solution, which further increases the solubility of TCP and enhances resorption. The presence of micropores in the sintered material can increase the solubility of these phases (Davis, 2004).

Sintering of calcium phosphate cerarnics usually occurs in the range of 1000 to 1500 ºC following compaction of the powder into the desired shape. The phases formed at high temperature depend not only on temperature but also the partial pressure of water in the sintering atmosphere. This is because with water present, HA can be formed and is a stable phase up to 1360 ºC. Without water, C_4P and C_3P are the stable phases. The temperature range of stability of HA increases with the partial pressure of water, as does the rate of phase transitions of C_3P or C_4P to HA. Due to kinetics barriers that affect the rates of formation of the stable calcium phosphate phases, it is often difficult to predict the volume fraction of high-temperature phases that are formed during sintering and their relative stability when cooled to room temperature (Yong et al., 1999).

Starting powders can be made by mixing in an aqueous solution the appropriate molar ratios of calcium nitrate and ammonium phosphate, which yields a precipitate of stoichiometric HA.

The Ca^{2+}, PO_4^{3-} and OH^- ions can be replaced by other ions during processing or in physiological surroundings; for example, fluorapatite, $Ca_{10}(PO_4)_6(OH)_{2-x}$ with $0 < x < 2$; and carbonate apatite, $Ca_{10}(PO_4)_6(OH)_{2-2x}(CO_3)_x$ or $Ca_{10-x+y}(PO_4)_{6-x}(OH)_{2-x-2y}$, where $0 < x < 2$ and $0 < y < ½x$, can be formed. FIuorapatite is found in dental enamel, and hydroxyl-carbonate apatite is present in bone (Pillar, 1990).

The mechanical behavior of calcium phosphate ceramics strongly influences their application as implants. Tensile and compressive strength and fatigue resistance depend on the total volume of porosity. Porosity can be in the form of micropores (<1 μm diameter, due to incomplete sintering) or macropores (> 100 μm in diameter, created to permit bone growth) (Cook et al.,1988).

The bonding mechanisms of dense HA implants appear to be very different from bioactive glasses. A cellular bone matrix from differentiated osteoblasts appears at the surface, producing a narrow, amorphous, electron-dense band only 3 to 5 μm wide. Between this area and the cells, collagen bundles are seen. Bone mineral crystals have been identified in this amorphous area. As the site matures, the bonding zone shrinks to a depth of only 0.05 to 0.2 μm. The result is normal bone attached through a thin epitaxial bonding layer to the bulk implant. Transmission electron microscope image analysis of dense HA bone interfaces has shown an almost perfect epitaxial alignment of the growing bone crystallites with the apatite crystals in the implant. A consequence of this ultrathin bonding zone is a very high gradient in elastic modulus at the bonding interface between HA and bone. This is one of the major differences between the bioactive apatites and the bioactive glasses and glass ceramics.

Resorption or biodegradation of calcium phosphate ceramics is caused by: physiochemical dissolution, which depends on the solubility product of the material and local pH of its environment; physical disintegration into small particles due to preferential chemical attack of grain boundaries; and biological factors, such as phagocytises, which causes a decrease in local pH concentrations. All calcium phosphate ceramics biodegrade at increasing rates in the following order:

α-TCP > β-TCP >> HA

The rate of biodegradation increases as:

- Surface area increases (powders > porous solid> dense solid)
- Crystallinity decreases
- Crystal perfection decreases
- Crystal and grain size decrease
- Ionic substitutions of CO_3^{2-} Mg^{2+} and Sr^{2+} in HA increase

Factors that tend to decrease rate ofbiodegradation include:

- F^- Substitution in HA

- Mg^{2+} substitution in β-TCP
- Lower β-TCP/HA ratios in biphasic calcium phosphates (Davis, 2004).

Different kinds of biomaterials used in human body are summarized in Figure 2.4 (Hench, 1985).

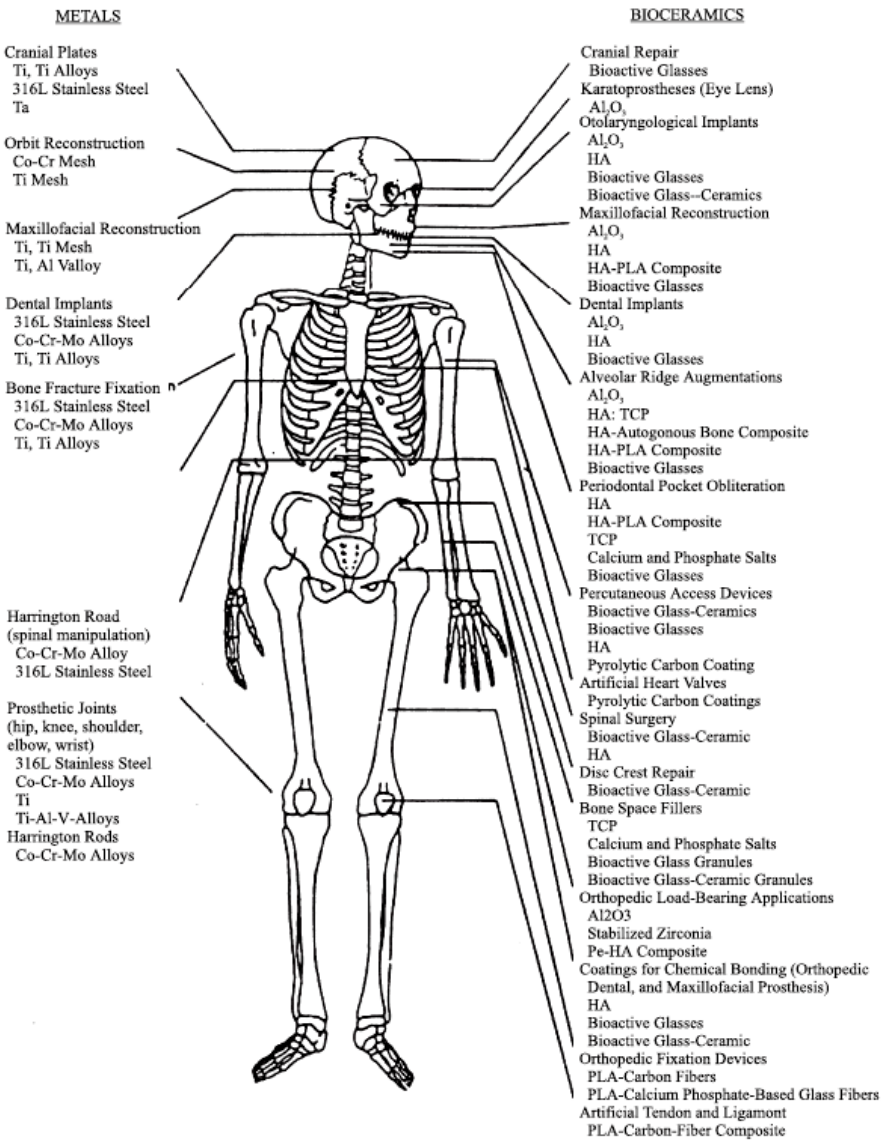

Figure 2.4 Clinical uses of inorganic biomaterials (Hench 1985).

CHAPTER THREE
COATINGS

3.1 Bioactive Coatings From Hydroxyapatite and Related Materials

A bio-active material that has attracted considerable interest is hydroxyapatite, which is a form of calcium phosphate. Calcium phosphate, i.e., hydroxyapatite, is a major constituent of bone, a metal implant that is coated with hydroxyapatite and placed inside bone does show rapid growth of bone cells into the hydroxyapatite coating. Once the growth of the bone cells is complete, the coated metal becomes very strongly bonded to bone. The coated apatite may eventually be resorbed by the body, which would in the long-term leave bare metal in contact with the bone (Savarino, Fini et al., 2003). Hydroxyapatite is non-toxic but advanced coating techniques are required to bond a strongly adhering coating to a metal.

Excessive roughness of the coated apatite inhibits bone regrowth while particles of coating may become detached and inhibit bone regrowth (Savarino, Fini et al., 2003). After regrowth of the bone around the implant, bone-to-implant bond strengths of the order of 10 MPa in shear and somewhat less than this in tension are reported (Milthorpe, 2000). This is less than the maximum tensile strength of cortical bone, but comparable to the tensile strength of cancellous bone (Milthorpe, 2000). Pull-out is a more likely mode of failure for a bone implant than bone fracture, even with a bio-active coating. Pull-out may not necessarily occur at the interface between bone and coating but instead between the metal and the hydroxyapatite coating. The brittleness of hydroxyapatite and its poor adhesion to metal compromise its performance as a coating (Redepenning et al., 2003).

Bio-active coatings based on hydroxyapatite have poor friction and wear properties (Fu et al., 1999), so these coatings should not be exposed to sliding movement. Sliding movements include microscopic motion (fretting) that typically occurs between tightly fitting surfaces.

Pure hydroxyapatite coatings are now being substituted by chitosan/hydroxyapatite composites (Redepenning et al., 2003) to improve bone adhesion or by fluorohydroxyapatite coatings to improve bone integration (Savarino, Fini et al., 2003). Finally, bioactive coatings of hydroxyapatite are not only used for orthopaedic implants but also as a component of temporary porous structures called 'scaffolds' for bone restoration (Maquet et al., 2003).

3.2 Coating Techniques For Applying Calcium Phosphates On Metallic Implants

There are several techniques for preparing hydroxyapatite coatings on metallic implant materials. Physical techniques used for processing hydroxyapatite coatings include vacuum plasma spraying, atmospheric plasma spraying, detonation-gun spraying, thermal processing, radio frequency magnetron sputtering, direct current magnetron sputtering, electron beam evaporation, pulsed laser deposition, ion beam sputtering, ion-beam assisted deposition, simultaneous vapor deposition, and plasma spraying. Chemical methods, including sol–gel, immersion coating, hot-isostatic pressing, electrophoretic deposition, electrochemical deposition, (micro)-emulsion routes, dip coating, sintering, and frit enameling, have also been used (Koch et al., 2007)

Plasma spraying is the most commonly used technique, depositing hydroxyapatite as a porous coating well suited to the ingress of bone cells [Kweh et.al, 2000]. A hot, highvelocity gas plasma is charged with a metallic powder and directed at appropriate regions of an implant surface. The powder particles fully or partially melt and then fall onto the substrate surface, where they solidify rapidly to form a rough coating (Schroeder et al., 1981).

For most plasma-spray processes, the temperature range of the plasma is 6600 – 11000 ºC (Whitehead et al., 1993). HA decomposes at 1300 ºC (Klein et al., 1994). It should be noted however that high temperature decomposition during plasma spraying impede the deposition of hydroxyapatite coatings and other deposition

processes such as electrostatic spray deposition may be more suitable [Leeuwenburgh et al., 2003]. Microstructure, crystallinity, and phase composition of HA coating is critical in deciding its cell response and mechanical performance. Plasma sprayed HA coating often result in the generation of secondary phases such as tricalcium phosphate (TCP), tetracalcium phosphate (TTCP), calcium oxide (CaO), and amorphous calcium phosphates (ACPs) (Lima et al., 2005). Though HA is very stable in the body environment, presence of secondary phases causes dissolution leading to degradation of the implant in vivo. In general the high temperature in this process decreases the degree of crystallinity of the coating. For example, the amorphous hydroxyapatite phase, which generally makes up between 5% and 20% of plasma-sprayed coatings, degrades much more rapidly than the crystalline hydroxyapatite phase. Hence, higher crystallinity content is required for the increased implant life. Heat treatment after plasma spray procedure can increase the crystallinitiy of the coating (Klein et al., 1994). The increased crystallinity, which is caused by the re-crystallization during heat treatment, may promote the stability of the coating.

In addition, plasma sprayed coatings contain large numbers of molten particles, defects, porosities, and cracks, which act to degrade coating integrity. Furthermore, plasma-sprayed coatings also contain stresses that result from the large coefficient of thermal expansion (CTE) mismatch between the hydroxyapatite coating and the metal substrate. For example, the CTE mismatch between hydroxyapatite (15×10^{-6} K^{-1}) and Ti 6Al–4V alloy (8.8×10^{-6} K^{-1}) is significant (Lu et al., 2004). In addition, plasma spraying of many metals and all polymers is precluded due to the high processing temperatures. As a result, a high proportion of plasma-sprayed hydroxyapatite coatings exhibit mechanical failure at the coating–substrate interface (Sun et al., 2001). From the economic point of view, the plasma spray process is also relatively expensive since HA powder in pure form is required.

Briefly, plasma spraying is the most frequently used coating- deposition technique because of the high reproducibility and economic efficiency of the process. Disadvantages of this process are poor mechanical properties due to the relatively

high thickness, poor adherence of the coating to the substrate, and the high-temperature deposition process, which causes problems with the integrity of the HA structure and composition. There are several drawbacks to this process, which include poor adhesion, nonuniform thickness, poor crystallinity, poor integrity, uneven resorption, mechanical failure at the coating/substrate interface, and increased implant wear (Hamdi et al., 2000).

A novel alternative technique that may eliminate the problems associated with the plasma spray process is the electrodeposition process (Shirkhanzadeh, 1995). The electrodeposition method is a low-temperature process using aqueous electrolytes which is prepared by dissolving reagent-grade $Ca(NO_3)_2$ and $NH_4H_2PO_4$ in deionized water.

Compared with plasma spray, electrochemical deposition has unique advantages due to its capability of forming uniform coating and simple setup. In addition, the deposition processing can be conducted at room temperature and the morphology of coating can be controlled easily by varying the electrochemical potential and electrolyte concentration (Kuo & Yen, 2002). However, the tear strength of HA coating produced by electrochemical deposition is much lower than that by the plasma spray. Some researchers have demonstrated that the addition of ethanol (Wang et al., 2003) or H_20_2 (Zhao et al., 2002) to the electrolyte solutions could improve the mechanical properties of HA coating. HU et al. (2002) prepared hybrid bioceramic coatings of HNpoly (vinyl acetate) on Ti-6A1-4V alloy, which exhibited a better tear strength.

It has been shown that the calcium phosphate coatings prepared by this method are uniform and adherent. It has also been seen that this process aIlows porous surfaces to be coated uniformly without clogging the pores. This effect can enhance the bone tissue growth and can also eliminate meta1 ions which may act as calcitication inhibitors (Shirkhanzadeh 1998).

The main advantage of the technique is that the chemical composition and crystal structure of the coatings can be easily controlled by varying the ion concentrations of the electrolyte. Since the chemical composition and crystal structure of the precipicated phases are dependent on the process paramerers such as the ion concentrations and the pH of the electrolyte, calcium phosphate coatings with desired chemical composition and rnicrostructure can be fabricated for specific applications. For example, calcium phosphate porous coatings fabricated at $[Ca^{2+}]$=20mM can provide relatively large surface areas which are particuIady desirable for effective adsorption and immobirization of proteins and amino acids (Shirkhanzadeh, 1994). The same author has reported the adsorption and immobilization of L-lysine into the above coatings as a method of fabricating delivery systems for sustained release of osteoinductive proteins. It has also been shown that at very low ion concentrations ($[Ca^{2+}]$=0.61mM) fine-grained hydroxyapatite can be obtained (Shirkhanzadeh, 1998). Fabrication of pure and fine grained hydroxyapatite coatings suitable for medical application is of great significance. Grain size reduction can greatly improve materials' properties. The small grain size allow for more efficient deformation mechanism (e.g. diffusion creep) and more effective crack dissipation than is normally available in coarse-grained ceramics (Siegel et al.,1988).

Shirkhanzadeh (1998) studied the significance of the pH during electrodeposition of calcium phosphate coatings and reported that marked changes in the morphology and crystal structure of calcium phosphate deposits were observed as the adjusted pH values of the electrolyte increased from 4.2 to 6.0. At acidic pH values (pH~4.2) the deposits consisted of a network of relatively large plate-like crystals in the range of 4-6 μm and deviated markedly from stoichiometric hydroxyapatite. These coatings exhibited apatite characteristics similar to bone apatite and non-stoichiometric hydroxyapatite. Previous work of Shirkhanzadeh (1995) has also found that calcium phosphates coatings prepared under the same conditions (pH~4.2) were uniform, adherent and had a thickness of about 80 μm. The coatings were found to be octacalciuum phosphate (OCP) type apatite and contained acid phosphate groups, Steam treatment followed by calcining at 425 ºC or a post treatment in alkaline solutions was necessary to convert these coatings into pure hydroxyapatite coatings.

Electrophoretic deposition of HA on metal substrates has been studied in an attempt to achieve uniform distribution of fine HA deposits. The advantages of this technique are high purity of layers formed, ease of obtaining the desired thickness, and strong layer adhesion to the substrate. The bond strength of the coatings is achieved by sintering; thus, shrinkage and cracking of the coating might occur during this process (Eliaz et al., 2005).

Pulsed laser deposition is a processing technique in which thin films are created through the energetic condensation of atomic and molecular species. This technique provides several advantages for the growth of hydroxyapatite and other ceramic materials (Cotell et al., 1994). Sputtering (Hulshoff et al., 1995; Yamashita et al., 1996) has the advantage of depositing thin coatings with a strong adhesion and compact microstructure. The deposition gas and the deposition temperature play key roles in determining the phase and crystallinity of calcium phosphate thin films obtained using pulsed laser deposition.

The sol-gel process is a simple and cheap method to obtain coatings of micrometer dimensions. Moreover, it has been reported that the materials prepared by sol-gel deposition are more bioactive than those prepared by other methods (Haddow et al., 1996; Li & Groot, 1994). Some hydroxyl (Ti-OH and Si-OH) groups remain on the coating, providing sites for calciumphosphate nucleation and then bone regeneration.

3.3 Functionally Graded Coatings Based on Calcium Phosphates

Functionally graded materials (FGMs) have a gradient compositional change from the surface to the interior of the material. With the unique microstructure of FGMs, materials for specific function and performance requirements can be designed (Wang et al., 1998). In the field of biomaterials, several approaches exist for the deposition of functionally graded coatings (FGCs) based on calcium phosphate compounds onto titanium alloy surfaces. Although still in the developmental stage, FGCs are being widely studied.

Figure 3.2 shows a calcium phosphate FGC graded in accordance to adhesive strength, bioactivity, and bioresorbability. Calcium phosphates have different phases. Hydroxyapatite has excellent chemical bonding ability with natural bone. Tricalcium phosphate (TCP), known in its two polymorphs of (α-TCP and β-TCP, is a biosorbable ceramic that dissolves gradually in body fluid, and new bone will eventually replace it. The solubility of (α-TCP is higher than that of β-TCP.)

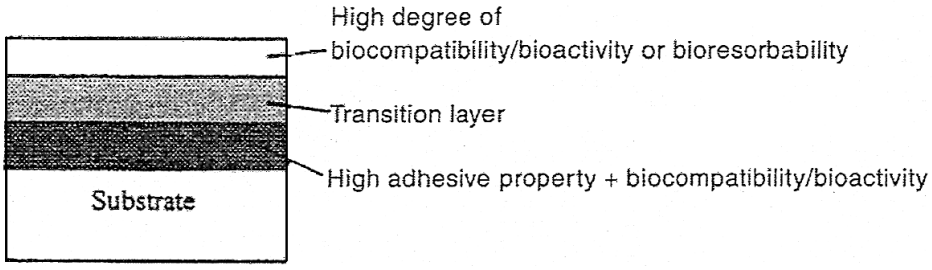

Figure 3.2 Calcium phosphate functionally graded coating (Wang et al., 1998).

CHAPTER FOUR
HARD TISSUE – BIOMATERIAL INTERACTIONS

4.1 Introduction: Bone As a Functional Organ

Bone and its several associated elements - cartilage, connective tissue, vascular elements, and nervous components - act as a functional organ. They provide support and protection for soft tissues and act together with skeletal muscles to make body movements possible. Bones are relatively rigid structures and their shapes are closely related to their functions. Bone metabolism is mainly controlled by the endocrine, immune, and neurovascular systems, and its metabolism and response to internal and external stimulations are still under assessment.

Long bones of the skeletal system are prone to injury, and internal or external fixation is a part of their treatment. Joint replacement is another major intervention where the bone is expected to host biomaterials. Response of the bone to biomaterial intervenes with the regeneration process. Materials implanted into the bone will, nevertheless, cause local and systemic biological responses even if they are known to be inert. Host responses with joint replacement and fixation materials will initiate an adaptive and reactive process (Santavirta et al., 1992)

The objective of this chapter is to review the tissue response to biomaterials implanted into the bone for a better understanding of interactions of the hard tissue and the implant. Metals, ceramics, and polymers and/or their composites and coatings are evaluated for their tissue response. The spectrum of response with metals lies between aseptic loosening and carcinogenesis. Ceramics, on the other hand, may cause a nonspecific inflammation and bone marrow depletion. Hydroxyapatite and calcium phosphate particles are shown to be capable of stimulating the expression and secretion of cytokines and proteases that enhance bone resorption. Polymethylmethacrylate and polylactide and/or polyglycolide materials are frequently used polymers in hard tissues. Extensive research on

improving the biocompatibility of these polymers used in clinical applications is going on. Various factors such as the type, structure, origin, and composition define the foreign body reaction toward the polymer. Polyhydroxybutyrate (PHBV) seems to cause a milder tissue response when compared with other polymers. Implants of metal should be of low profile, and their properties should be improved to overcome wear debris. Less use of metals for bone and joint replacement in the future is expected (Santavirta et al., 1992).

4.2 Metals

4.2.1 Biocompatability

Metals have been used successfully for decades in fracture fixation and joint replacement. Mechanisms of implant failure were recently the target of intensive research as longevity and expectations from such implants are increasing (Praemer et al., 1992). An estimated 11 million people in the United States reported having at least one medical device in 1988 (Praemer et al., 1992). Fixation devices and artificial joints comprise 44% of all medical devices. The percentage of usage of fixation devices and artificial joints with one or more problem were 33.2 and 31.6%, respectively (Praemer et al., 1992). The demand for such medical device implants is expected to increase in the coming years.

Currently used metal implants are expected to be inert when implanted into the human bone. They are supposed to be bioactive as their surfaces are porous or coated. Metallic fixation devices are usually used alone, whereas artificial joints can comprise several parts other than metal including polymer and ceramic. If only metal has been used as in the case of uncemented endoprostheses, in a young and active patient, the head of the prosthesis may be bipolar. Cemented prostheses once again became popular using the third generation cementing techniques (i.e., medullary plug, centralizers, viscous cement, pressurising). It is obvious that the rate of complication will increase as the number of materials used in an artificial joint increases. The type of metal, manufacturer and its standards, alloy, composition,

processing conditions, and mechanical properties influence the interaction of metal and the bone. Stainless steel, cobalt, titanium, and their alloys are widely used in the production of artificial joints and fixation devices. The advantages of titanium over cobalt alloys are lower modulus of elasticity and higher biocompatibility (Head et al., 1995). The rate of reaction toward metals is more severe in artificial joint surgery than fracture fixation as motion in the prior and immobilization in the latter are the ultimate aims.

Long-term stability is closely related to bone–implant integration. Bone cells mediate initial response to the implant. The interaction between osteoblasts and biomaterial surfaces was evaluated extensively. Response of osteoblastic cells toward commonly used titanium and cobalt alloys revealed cellular extension on both alloys during the first 12 h (Shah et al., 1999). Osteoblasts spread relatively less on rough titanium alloy than cobalt alloy. Vinculin immunostaining at focal adhesion contacts distributed throughout the cells adhering to titanium alloy, but were relatively sparse and localized to cellular processes on cobalt alloy. Cell attachment was directly to implant materials through integrins (Gronowicz & McCarthy, 1996). Thus, the initial interaction between the implant and surrounding bone might differ to the origin of osteoblastic cells. Both titanium and cobalt alloys demonstrate good biocompatibility. Osseointegration was less on cobalt alloy surfaces though cartilage, and osteoid tissue was observed more frequently on the cobalt alloy than on the titanium alloy surface (Jinno, 1998). Cobalt alloys were also presented to release large amounts of metal ions, which could mediate cytokine release and hypersensitivity reaction (Granchi et al., 1999). Osseointegration established extensively when titanium was implanted into bone marrow. Thus, some bone marrow cells formed an incomplete layer in contact with the titanium implant and presented morphologic characteristics of macrophages and multinucleated giant cells (Rahal et al., 1993).

Clinical features of aseptic loosening in artificial joints are pain and loss of range of motion. Radiography reveals osteolysis at the bone–implant interface. Osteolysis can be recognized with cemented and uncemented implants. Osteolysis may be

asymptomatic in some patients with uncemented implants, demonstrating that osteolysis alone may not be of clinical importance and a sign of loosening. Osteolysis is known to increase with years of follow-up in cemented and uncemented implants (Boneli, 1994). In cemented implants, osteolysis may vary according to the type of cement and application procedure. Effect of bone cement on bone will be discussed in coming sections. It was found that most of the debris belonged to the ultra high molecular weight polyethylene (mean size, approximately 0.5 μm) of the acetabular cup in loose, uncemented artificial hip joints (Shanbhag et al., 1994). In cemented artificial hip joints, wear particles arise from the bone cement itself, acetabular cup polyethylene, and metal, respectively. Metal and polymer particles initiate the complex, biomaterial-initiated osteolytic and/or adaptive cascade (Fig. 4.1) in a size- and dose-dependent manner. Metal particles are also defined to cause apoptosis in cells of tissue around the implant (Stea et al., 2000). Numerous macrophages, foreign body giant cells, and fibroblasts generally surround abundant particle debris. Phagocytosis of debris by macrophages may serve as a stimulus for cellular activation with synthesis and secretion of bone-resorbing factors.

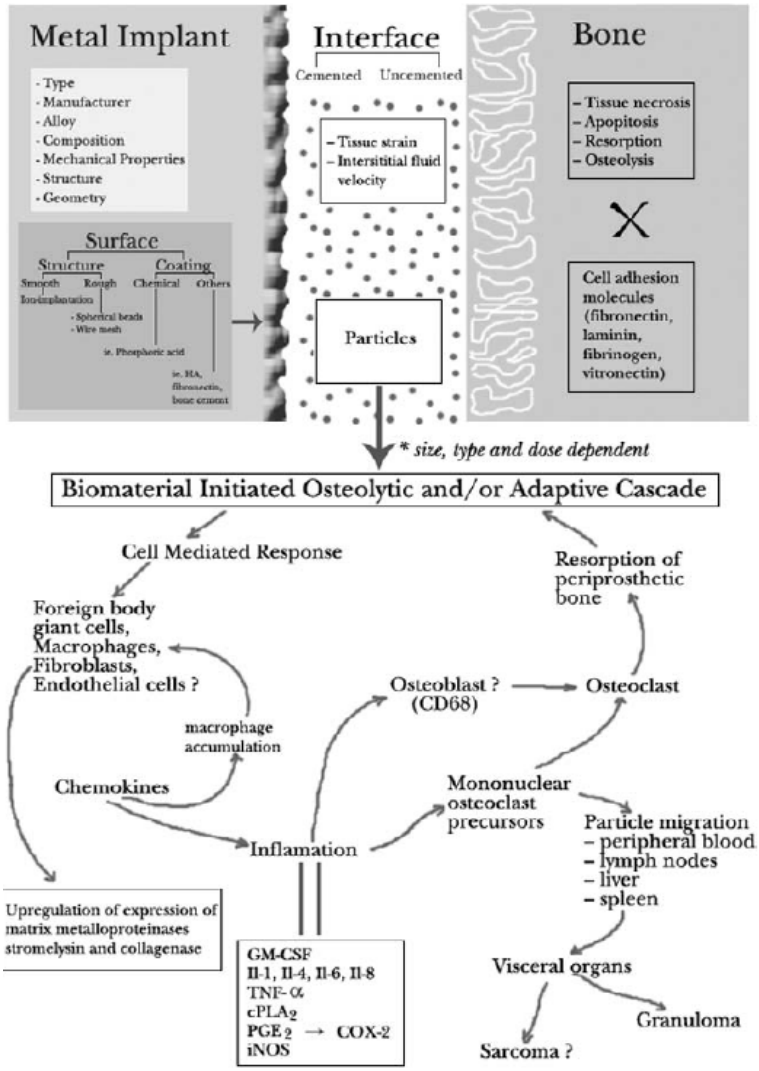

Figure 4.1 Metal implant–hard tissue interface and the biomaterial-initiated osteolytic and/or adaptive cascade (Michael et al., 2004).

4.2.2 Effectiveness of Metal Coatings

Coatings or ion implantation (Sovak et al., 2000) are usually used to improve the biocompatibility of implants and decrease metallic wear and corrosion. Rough or porous surfaces allow cell attachment. One simple method to allow tissue ingrowth into the implant is to modify its surface by implanting spherical beads (Hofmann et al., 1997) or wire mesh. Though manufacturers' manuals indicate these surface modifications allow bone cells to grow into the implants and increase their mechanical strength and biocompatibility, longitudinal, randomized, prospective clinical studies with longterm follow-up are lacking. A case report concerning bone

ingrowth in a porous-coated knee arthroplasty revealed that the prosthesis was held in situ by collagenous tissue, and calcified bone did not appear to interact with the metallic coating. One in vitro experimental study, on the other hand, revealed that rough Ni-Ti surface promoted transforming growth factor beta (TGF-β) expression, a mediator of bone healing and differentiation (Kapanen et al., 2002). Another autopsy study of five femurs indicated that circumferential porous coating of uncemented femoral components could prevent distal migration of polyethylene wear debris (von Knoch et al., 2000).

An alternative method is the use of biocompatible chemicals and materials such as ceramics for coating. Titanium surfaces were modified using phosphoric acid in an in vitro study to improve the biocompatibilty of dental implants. Results indicated that pretreatment of the implant with phosphoric acid caused no cytotoxicity to the osteoblasts (Viorney et al., 2002). Micro arc oxidation method in phosphoric acid on titanium implants provided chemical bonding sites for calcium ions during mineralization (Sul et al., 2002). Hydroxyapatite (HA) coating is a proven method to improve the implants' mechanical bonding (Cook et al., 1988) and biocompatibility (Dalton et al., 1995). It is demonstrated that when the gap between the coating and bone is 1.0 mm or less, mechanical attachment strength and bone ingrowth increase significantly at all time periods. Alkaline phosphatase activity, a marker of osteogenic activity, increases significantly with respect to the uncoated titanium in hydroxyapatite-coated implants (Montanaro et al., 2002). The quality and thickness of coating may vary between manufacturers, and thick coatings on metal surfaces are prone to delamination. Bone ingrowth and attachment mainly take place on the distal and medial parts of the HA-coated surface of femoral implants (Coathulp et al., 2001).

4.3 Ceramics

Ceramics used in orthopedic surgery and traumatology as bone tissue substitutes are mainly of hydroxyapatite, tricalcium phosphate (TCP), or glass ionomer origin. Ceramics can be categorized as (1) fast-resorbing, (2) slow-resorbing, and (3)

injectable ones (Koc & Timucin, 1999). Ceramic composites have found their place in promoting healing of bone in clinical practice alone or in combination with other materials with their osteogenic, osteoconductive, and/or osteoinductive properties. These ceramics can also be used as carriers of bone cells, growth factors (Takaoka et al., 1988), or drugs (Krajewski et al., 2000) such as antibiotics (Shinto et al., 1992) and anticancer medicine (Uchida et al., 1990). Advantages of ceramics over metals are their favorable bioactivity and interaction with the host tissue. Bioactivity of ceramics is mainly limited to osteoconduction as long as they do not carry cells and/or growth factors. Thus, clinical and basic research results lack a detailed understanding of these materials' exact biological effects.

The ultimate aim of porous degradable ceramics implanted into bone is natural organ replacement at load-bearing or void-filling sites. Normal tissue interacting with these ceramics is supposed to replace the implant in time. Tricalcium phosphate is known to degrade more rapidly than HA and is used in non-weight-bearing sites. The degradation rate of HA and TCP may change depending on the manufacturer, pore size, porosity, composition, and sintering temperature. The rate of degradation per year of TCP and HA is about 35 and 1–3%, respectively. One recent study, however, indicates that TCP degradation does not occur even after 6 months and a thin fibrous layer surrounds the nonloaded ceramic at all times. Mechanical properties of hydroxyapatites in general were superior compared to TCP. However, bending and torsional stresses may fracture HA easily (Balcik, 2002).

Apatite ceramics of natural and synthetic origin, allogenic bone chips, and calcium carbonate are also frequently used in dentistry. One study (Gurmeric, 1995), compared the effects of these ceramics in defects created in the mandible of mongrel dogs (Fig. 4.2).

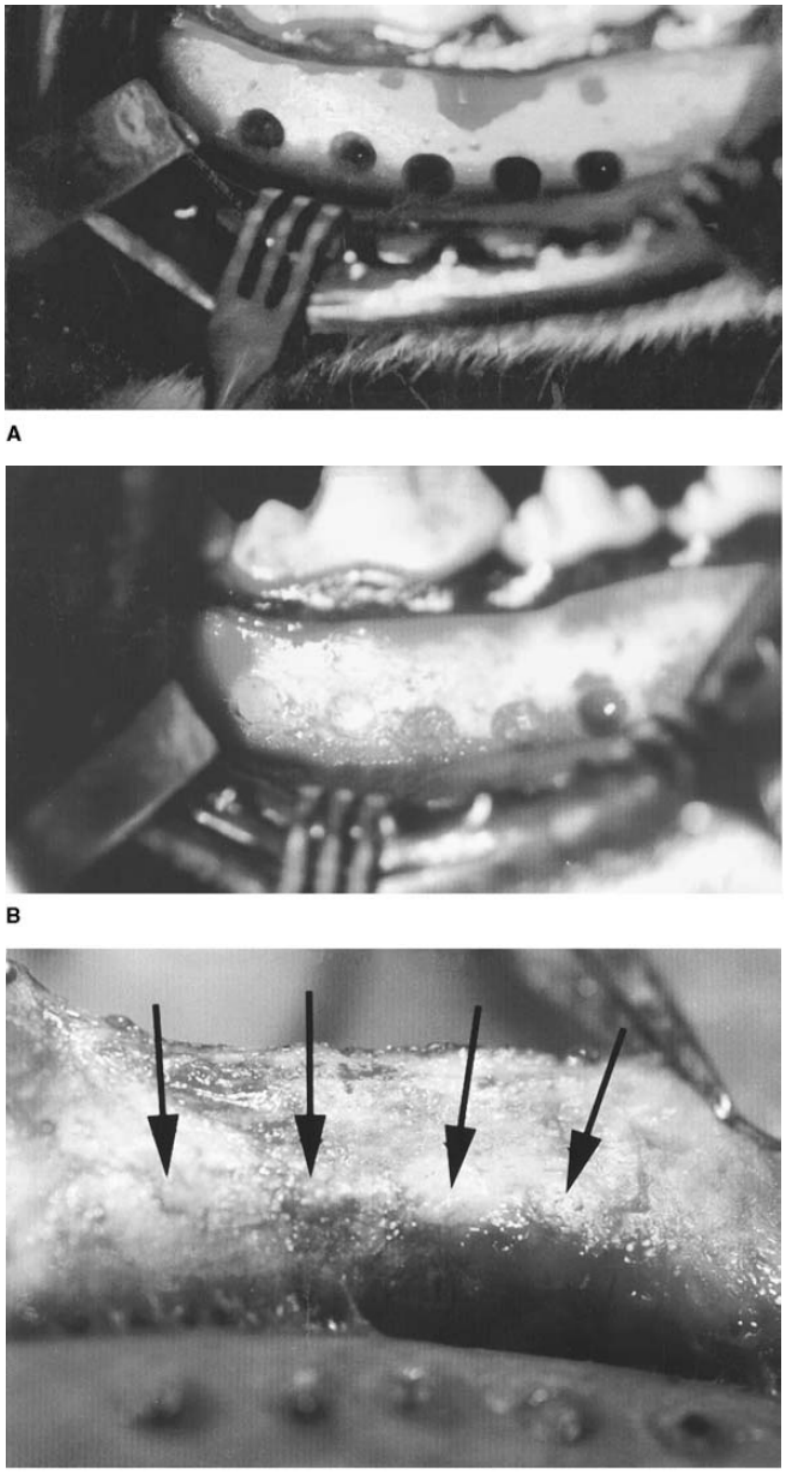

Figure 4.2 From left to right: control, allogenic bone chips, natural apatite ceramic, synthetic hydroxyapatite, and calcium carbonate implantation into the mandible of mongrel dogs. (A) cavities opened in the mandible; (B) biomaterial implantation; and (C) macroscopy at 4-week follow-up. Also note periosteal reaction at sites where biomaterials were in contact with the implants (Gurmeric, 1995).

The results of that study indicate in 1 week natural apatite of coral origin established loose connective tissue with some osteoblasts adjacent to it (Fig. 4.3). Natural apatite resorbed in 4 weeks leaving its place to bone trabecules. Active osteoclasts were observed in the newly establishing Haversian system. Foreign body reaction and inflammation was not observed with natural apatite. Only granules detached from the coral elucidated fibrous encapsulation and osteoclastic activity. In 1 week, calcium carbonate disappeared totally leaving a cavity of granulation tissue. Some osteoblasts were observed at the bone–cavity border. In 4 weeks, the granulation tissue was replaced by dense connective tissue. Findings were inferior with calcium carbonate than coral apatite. Dense connective tissue also established with synthetic apatites; however, osteoblastic activity with these ceramics at the implant–bone interface was better than that of calcium carbonate. Thin new bone trabecules were surrounding the synthetic HA in some locations. Synthetic HA presented a favorable bonehealing sequence, with no foreign body reaction and osteoclasts at 1 week when compared to the other materials (Fig. 4.4). New bone did not grow well in cavities where allogenic bone chips were implanted. Bone healing was always from the peripheral to the central part of the implant. All implants presented an osteoconductive property. Reaction to these implants by bone was limited probably due to the dense cortical structure of the mandible. Best results were attained with natural apatite followed by synthetic apatite (Fig. 4.5). Allogenic bone chips and calcium carbonate followed (Fig. 4.6) these two materials in effectiveness means of bone healing. Hydroxyapatite particles in the periosteum elaborated a significant osteoclastic activity (Fig. 4.7) (Gurmeric, 1995). Thus, bone healing of the mandible is known to be significantly better than of the femur of rabbits (Tassery, 1999).

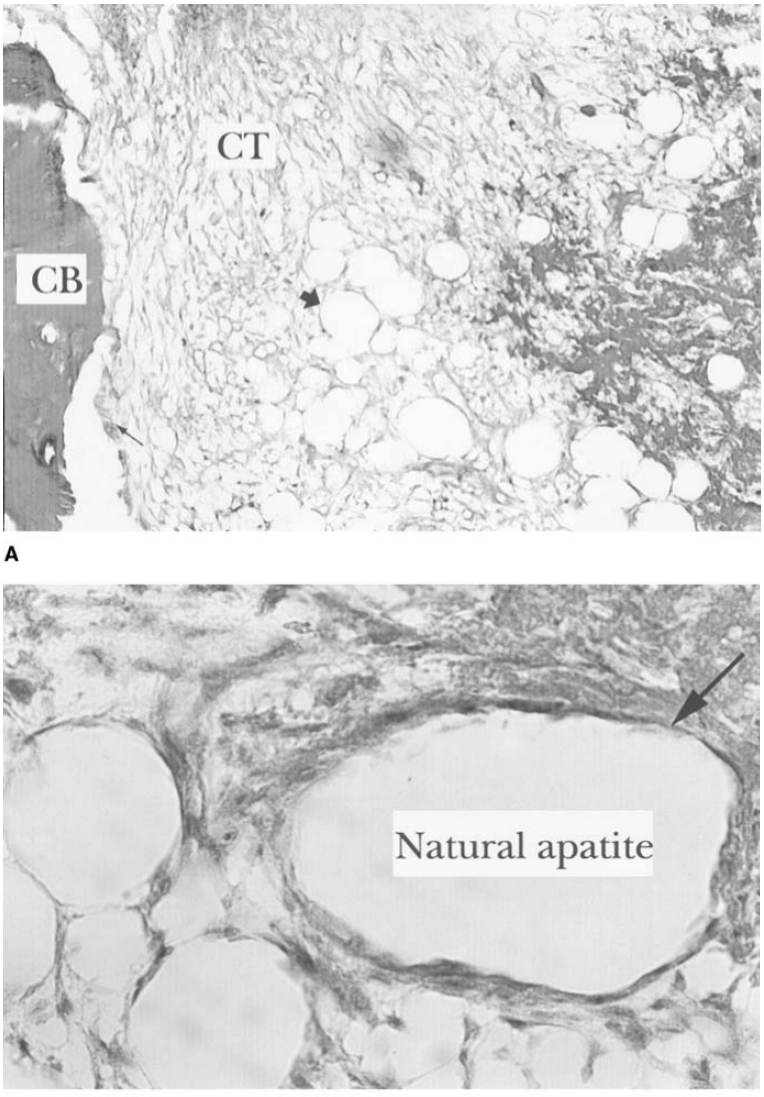

Figure 4.3 Natural apatite of coral origin. (A) Cellular connective tissue (CT) in between cortical bone (CB) and implant containing minimal osteoblasts at week 1. Arrow indicates voids of cavities belonging to the implant. Massons Trichrome 40X. (B) Voids of implant surrounded by fibrous connective tissue. HE 40X (Michael et al., 2004).

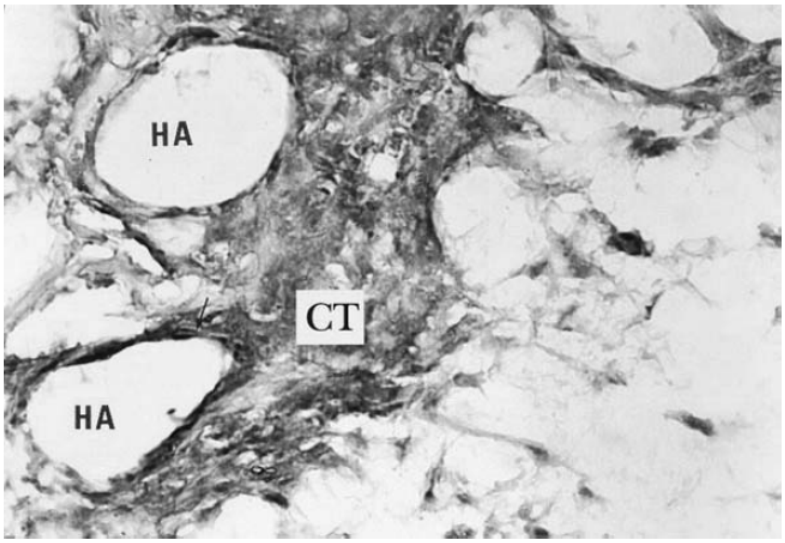

Figure 4.4 Synthetic HA. Favorable healing sequence without osteoclasts at week 1. Hydroxyapatite granules are surrounded by dense connective tissue (CT). HE 400X (Michael et al., 2004).

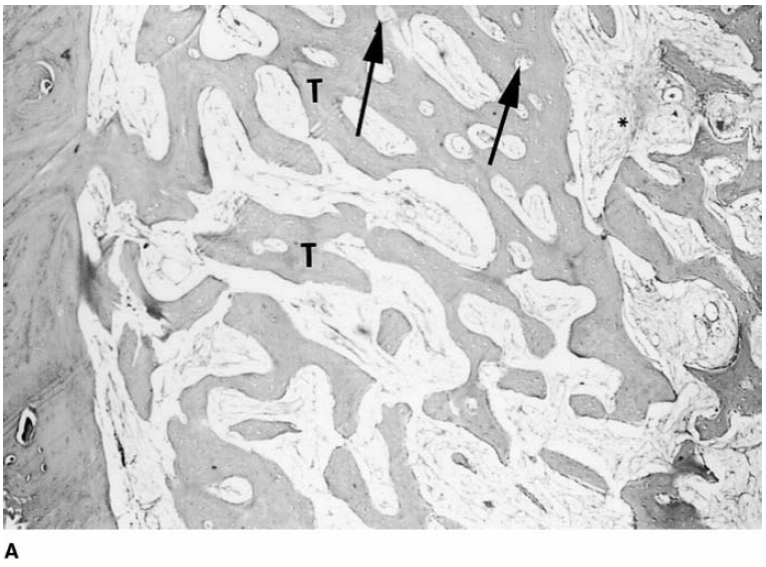

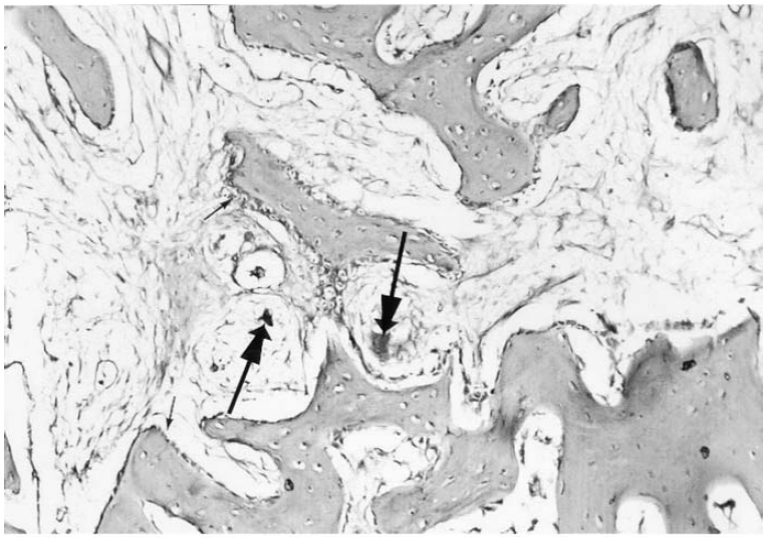

B

Figure 4.5 Synthetic hydroxyapatite. (A) New trabecular bone (arrows) healing at week 4. Arrows indicate the new establishing Haversian canals. HE 40X. (B) Osteoblasts and osteoclasts (arrows) can be seen around the new bone trabecules. HE 10X (Michael et al., 2004).

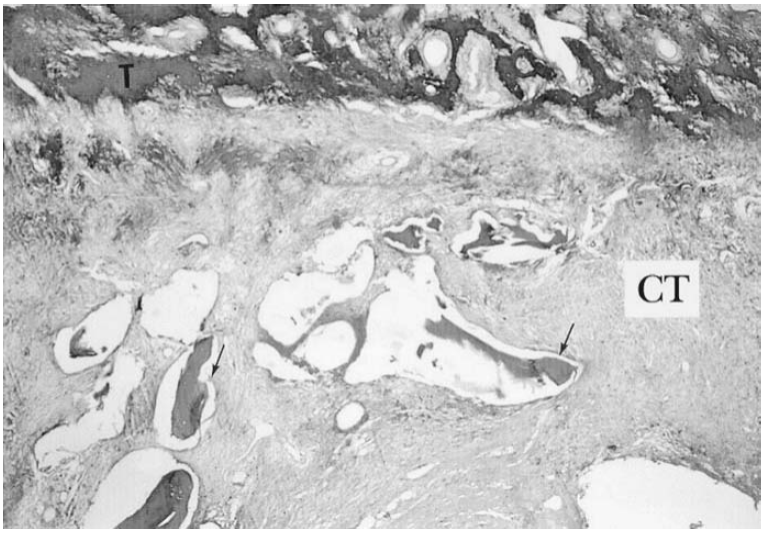

Figure 4.6 Allogenic bone chips. Dense connective tissue (CT) can be observed in close contact with the new bone trabecules. Trichrome 40X (Michael et al., 2004).

Natural ceramics are presented to be more effective in attracting cells and favoring their proliferation than synthetic ones. Large amounts of mineral powder may also down-regulate osteogenic markers such as alkaline phosphatase activity and osteocalcin release (Fig. 4.8) (Midy et al., 2001).

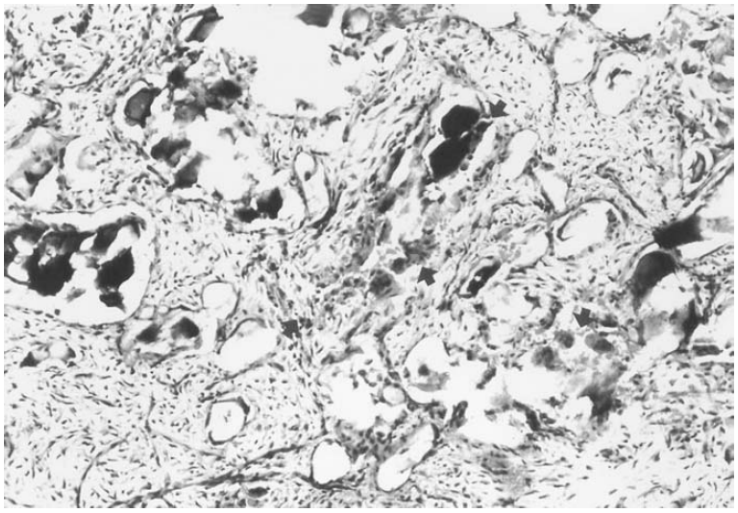

Figure 4.7 Hydroxyapatite particles in the periosteum elaborate significant osteoclastic activity. HE 100X (Gurmeric, 1995).

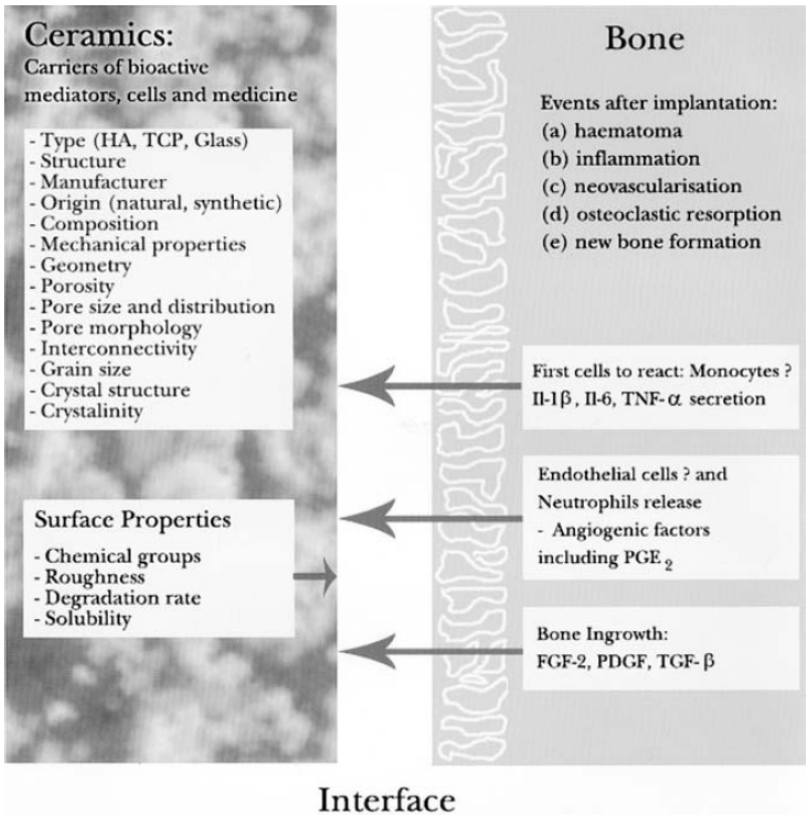

Figure 4.8 Ceramic implant–hard tissue interface (Midy et al., 2001).

CHAPTER FIVE
EXPERIMENTAL STUDIES

5.1 Purpose

The objective of this study was to form hydroxyapatite (HA) coatings on medical grade 316L Stainless Steel by using an galvanostatic electrochemical deposition technique which is applying at constant current and investigate the chemical composition and morphological structure of these coatings.

The phases of deposits were characterized by X-Ray diffraction (XRD) and Fourier transform infra-red spectroscopy (FTIR). Morphology of the coatings was investigated by scanning electron microscope (SEM). Ca/P atomic and weight and ratios calculated by energy dispersive spectroscopy (EDS) analysis and results compared with the quantitative analysis of crystalline components in the XRD patterns.

Experimental studies in this study are divided into two main parts:

Part 1. Electrochemical Deposition of Brushite on 316L SS and Its Conversion to Hydroxyapatite by NaOH Treatment: Aim of this part is form a homogenous brushite (DCPD) coating having different shapes and sizes of crystals on 316L stainless steel and transformation of DCPD coating to HA by NaOH alkali treatment. Effect of current density on the morphology and chemical composition of the coatings is one of the scopes of this part of the thesis.

Part 2. Electrochemical Deposition of Hydroxyapatite on 316L SS: In this part, we have tested the growth of HA films on 316L stainless steel by galvanostatic method in two different ion concentrations at 90^{o}C. A stable HA coating on 316L stainless steel in an aqueous solution was formed. The effects of the current density and the ion concentration on coating morphology, microstructure and composition were discussed.

5.2 Material and Sample Preparation

Implant quality 316L stainless steel is used in the field of implant surgery because of its relatively low costs, high machinability, and reasonable corrosion resistance but since it has some poor properties it requires applying some coatings to withstand dynamic loads and aggressive body fluids in human body. Chemical composition and microstructure of an implant quality 316L stainless steel used in this study are given in Table 5.1 and Figure 5.1 respectively.

Table 5.1 Chemical composition of 316L stainless steel.

Wt. % Element	**Cr**	**Ni**	**Mo**	**C**	**Mn**	**S**	**Si**	**N**	**Cu**	**Nb**	**P**	**Fe**
316L	17-20	1-17	2-4	0.03 max	2.00 max	0.03 max	0.03 max	0.75 max	0.10 max	0.50 max	-	Balance

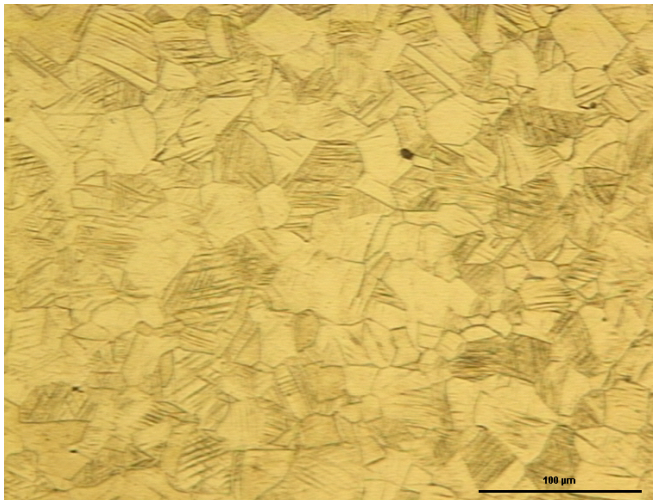

Figure 5.1 Microstructure of medical grade 316L etched in 42% HCI, 28% HNO_3, 28% Acetic Acid, 2% Glycerine solution (20X).

In this study, medical grade 316L stainless steel samples with 8 mm thickness and 16 mm in diameter were used as a substrate for coatings. Samples were first grinded with silicon carbide paper with decreasing surface roughness 80-240-400-800-1000-1200 grit and then polishing of samples were done with 6 µm and 3 µm diamond paste for obtain stretch free mirror like surface. Samples were cleaned in ultrasonic bath for 15 minutes before deposition.

5.3 Electrochemical Deposition of the Coatings

When a metallic salt is dissolved in water it dissociates to form positively charged ions. The solution that contains these charged ions is referred to as an electrolyte or a plating solution. By passing a sufficient amount of electric current through this electrolyte, one can reduce the metal ions to form solid metal. This process is most commonly referred to electroplating or electrochemical deposition (Schlesinger et al., 2000).

Electroplating is often also called "electrochemical deposition", and the two terms are used interchangeably. As a matter of fact, "electroplating" can be considered to occur by the process of electrochemical deposition. Electrochemical deposition is the process of producing a coating, usually metallic, on a surface by the action of electric current. The deposition of a metallic coating onto an object is: achieved by putting a negative charge on the object to be coated and immersing it into a solution, which contains a salt of the metal to be deposited (in other words, the object to be plated is made the cathode of an electrolytic cell). The metallic ions of the salt carry a positive charge and are thus attracted to the object. When they reach the negatively charged object (that is to be electroplated), it provides electrons to reduce the positively charged ions to metallic form. Figure 5.2 is a schematic presentation of an electrolytic cell for electroplating a metal "M" from an aqueous (water) solution of metal salt "MA".

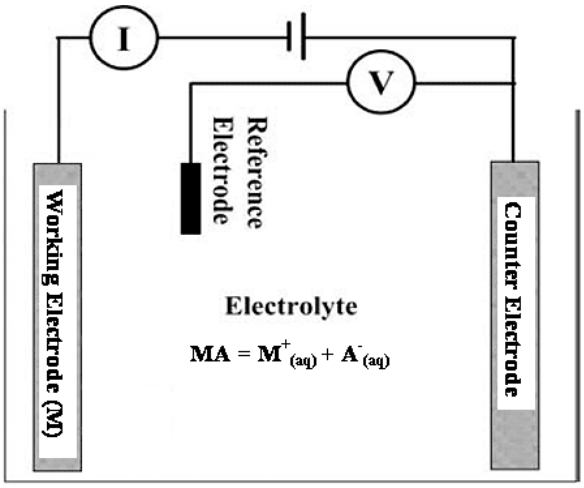

Figure 5.2 Schematics of an electrolytic cell for plating metal "M" from a solution of the metal salt.

5.3.1 Potentiostat/Galvanostat

A potentiostat is an electronic instrument that controls the voltage difference between a working electrode and a reference electrode. Both electrodes are contained in an electrochemical cell. The potentiostat implements this control by injecting current into the cell through an auxiliary, or counter, electrode. In almost all applications, the potentiostat measures the current flow between the working and auxiliary electrodes. The controlled variable in a potentiostat is the cell potential and the measured variable is the cell current.

Potentiostats can also be operated as a galvanostat. Galvanostat is an electronic instrument that controls the current through an electrochemical cell at a preset value, as long as the needed cell voltage and current do not exceed the compliance limits of the galvanostat. It also called "amperostat."

5.3.2 Electrochemical Cell

The electrodes are immersed in an electrolyte (an electrically conductive solution). The collection of the electrodes, the solution, and the container holding the solution are referred to as an electrochemical cell.

The electrodeposition process was carried out in an electrochemical cell. The schematic diagram of the cell is shown in Figure 5.3. The electrolytic cell was fitted with a saturated calomel electrode (SCE) positioned in a Luggin capillary acting as a reference electrode. A graphite rod was used as counter electrode. Medical grade 316L stainless steel (substrate) was used as the cathode for the deposition of calcium phosphate coatings. 316L S.S. samples were mounted in an epoxy-resin mould except metal surface and electrical connection between pincer and metal surface was provide by a copper wire that soldered back of the samples. The current of the cathode was maintained at a constant value by a Gamry PC-750/4 potentiostat/galvanostat in galvanostatic mode. Galvanostatic polarization method was applied for deposition of the coatings. At a constant current, potential variation

vs. SCE was measured as a function of time during the experiment. The electrolyte temperature was kept constant by a heater jacket surrounding the cell and a temperature controller probe of heater soaked in electrolyte.

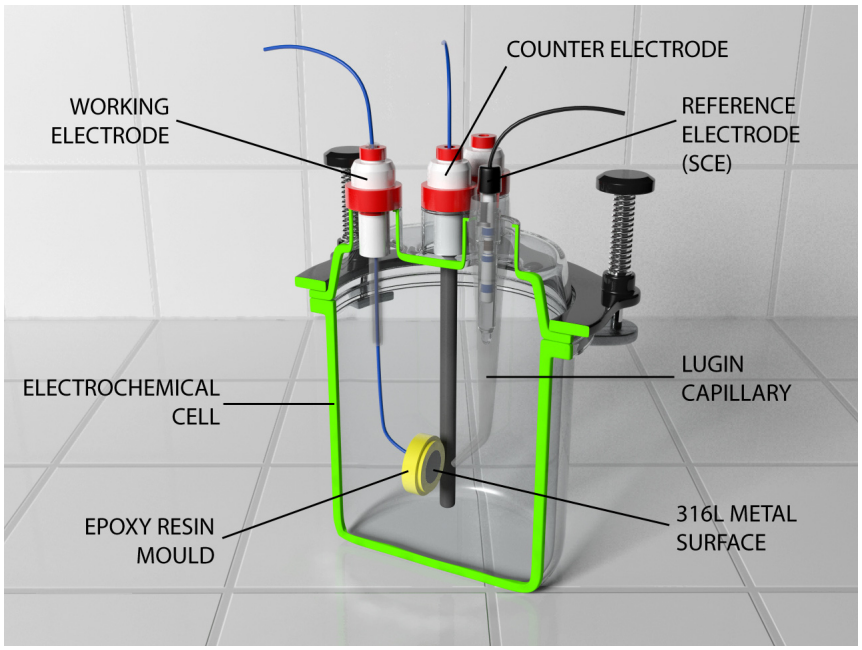

Figure 5.3 Three electrode electrochemical cell.

5.3.3 Electrodes

A potentiostat/galvanostat requires an electrochemical cell with three electrodes as shown in Figure 5.3.

5.3.3.1 Working Electrode

The Working Electrode (WE) is the electrode where the potential is controlled and where the current is measured. For many physical electrochemistry experiments, the Working Electrode is an "inert" material such as gold, platinum, or glassy carbon. In these cases, the Working Electrode serves as a surface on which the electrochemical reaction takes place. In corrosion testing, the working electrode is a sample of the corroding metal. In electrochemical deposition process, the working electrode is cathode which will be coated. Generally, the working electrode is not the actual metal structure being studied. Instead, a small sample is used to represent the

structure. This is analogous to testing using weight loss coupons or substrates for coating. The working electrode can be bare metal or coated.

5.3.3.2 Reference Electrode

The Reference Electrode (RE) is used in measuring the working electrode potential. A reference electrode should have a constant electrochemical potential as long as no current flows through it. The most common lab reference electrodes are the Saturated Calomel Electrode (SCE) and the Silver/Silver Chloride (Ag/AgCl) electrodes. In field probes, a pseudo-reference (a piece of the working electrode material) is often used.

The Saturated Calomel Electrode (SCE) is a reference electrode based on the reaction between elemental mercury and mercury(I) chloride. The aqueous phase in contact with the mercury and the mercury(I) chloride (Hg_2Cl_2, "calomel") is a saturated solution of potassium chloride in water (Figure 5.4).

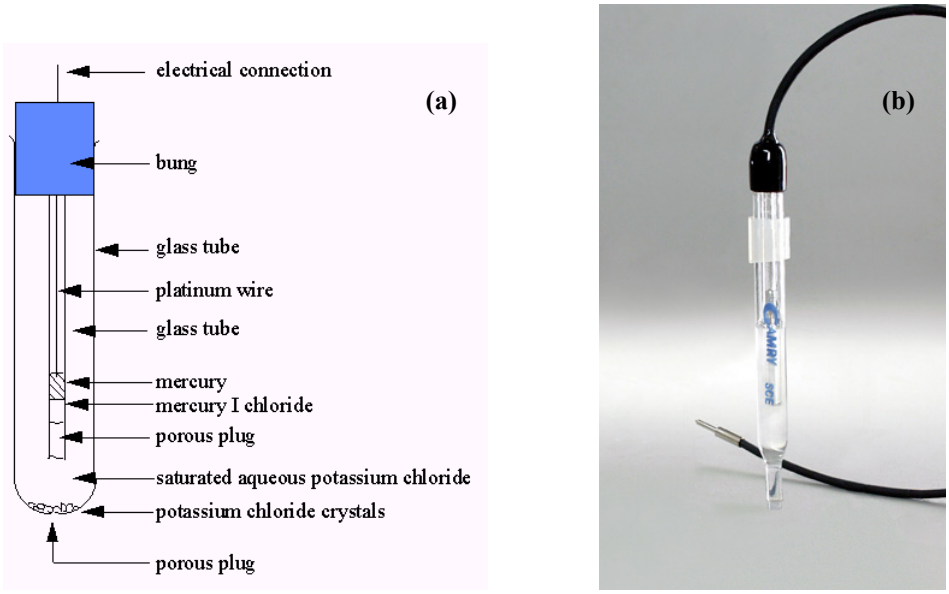

Figure 5.4 (a) Schematic view of SCE (b) SCE used in this study.

A Luggin Capillary is used to position the sensing point of a reference electrode to a desired point in a cell. The Luggin capillary in a laboratory cell is made from glass or plastic. It is generally filled with the test solution. The Luggin holds the reference electrode as shown in the picture above. The tip of the Luggin capillary

near the working electrode is open to the test solution. The reference electrode senses the solution potential at this open tip.

Note that the Luggin tip is significantly smaller than the reference electrode itself. The Luggin capillary allows sensing of the solution potential close to the working electrode without the adverse effects that occur when the large reference electrode is placed near the working electrode (Figure 5.5).

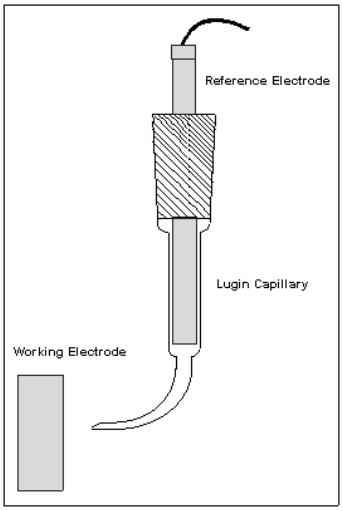

Figure 5.5 Schematic view of Luggin capillary.

5.3.3.3 Auxiliary (Counter) Electrode

The Auxiliary electrode is a conductor that completes the cell circuit. The auxiliary (counter) electrode in lab cells is generally an inert conductor like platinum or graphite. In field probes, it's generally another piece of the working electrode material. The current that flows into the solution via the working electrode leaves the solution via the auxiliary electrode.

5.3.4 Preparation of the Electrolytes

The electrolytes used for fabrication of CaP coatings was made by mixing 1 liter of 42 mM calcium nitrate 4-hydrate ($Ca(NO_3)_2 \cdot 4H_2O$) and 1 liter of 25 mM ammonium dihydrogen orthophosphate ($NH_4H_2PO_4$) solutions. Solutions were

prepared using analytical reagent grade chemicals and distilled water. Dilutes solutions with two different concentrations were prepared from the stock solution for the coating procedure. The calcium and phosphate ion concentrations of the electrolytes were diluted to 2.1 mM, 1.05 mM and 1.25 mM, 0.625 mM respectively respect to Ca/P ratio was 1.67. The pH of the electrolytes measured by bench top pH meter (Metler Toledo model MP225). Table 5.2 shows the concentrations and corresponding pH values at room temperature and at 90°C. The depositions were carried out at room temperature in electrolyte No.1 in the first part of this thesis. To show the effect of electrolyte temperature on the coating morphology and chemical composition the solutions were heated to 90°C and diluted electrolytes (Electrolytes No.2 and No.3) were used in the second part of the thesis.

Table 5.2 Calcium and phosphate ion concentrations and pH of the electrolytes at room and working temperatures.

Electrolyte Number	**$[Ca^{2+}]$ (mM)**	**$[H_2PO_4^-]$ (mM)**	**pH at 25ºC**	**pH at 90ºC**
1st Part				
No.1	42	25	4.15	3.94
2nd Part				
No.2	2.1	1.25	5.05	5.00
No.3	1.05	0.625	5.50	5.33

5.3.5 Coating Procedure

Calcium phosphate coatings were deposited on the 316L S.S. substrate by applying constant current in galvanostatic mode. The current density values used in the first and the second part of this thesis are -0.5, -5, -10 mA/cm^2 and -0.5, -1, -2.5 mA/cm^2, respectively. The substrate was immersed vertically in the electrolyte solution. Coatings were applied for varying time periods ranging from 3 minutes to 2 hours. Electrolytes weren't stirred and no other attempts were made to exclude CO_2 from the electrolyte. The substrates were removed from the cell after the deposition process was completed and were immersed in de-ionized water for 1 minute to wash away any trace of nitrate and calcium ions from the coating. The coating was then dried in a stream of hot air.

Deposition parameters used in two main parts of this study are given in table 5.3.

Table 5.3 Electrochemical deposition experimental parameters.

Electrolyte Number	Deposition Temperature (°C)	Current Density (mA/cm^2)	Deposition Time (s)	Total Charge (mC)
1st Part				
No.1	25	-0.5	3600	1800
No.1	25	-5	360	1800
No.1	25	-10	180	1800
2nd Part				
No.2	90	-0.5	7200	3600
No.2	90	-1	7200	7200
No.2	90	-2.5	7200	18000
No.3	90	-0.5	7200	3600
No.3	90	-1	7200	7200
No.3	90	-2.5	7200	18000

5.4 Morphological and Chemical Characterization Studies

5.4.1 Scanning Electron Microscope (SEM)

JEOL JSM-6060 Scanning Electron Microscopy (SEM) was used to examine the morphology of HA coatings.

5.4.2 Energy Dispersive Spectroscopy (EDS)

The regional elemental analyses of the specimens' surfaces by X-ray mapping of the coatings were observed with a 500 Digital Processing (IXRF Systems, Inc.) energy-dispersive X-ray spectroscopy (EDS) attached to the SEM. The regional elemental analyses of EDS measurements were performed at 1000X magnification to determine the Ca/P weight % and atomic ratios.

5.4.3 X-Ray Diffraction (XRD)

The crystalline structure of the coatings was determined by X-ray diffraction (XRD) Rigaku D/max-2200/PC with Cu-Kα radiation (0.02°/1s) and operated at a tube voltage of 40 kV and current of 20 mA.

5.4.4 Fourier Transform Infra-red Spectroscopy (FTIR)

Fourier transform infra-red (FTIR) spectroscopy was used to determine chemical composition of calcium phosphate phases. The FTIR spectra were recorded by using Perkin Elmer Spectrum BX spectrometer with attached thin film apparatus in transmission mode within the 4500-400 cm^{-1} wave number range.

CHAPTER SIX
RESULTS AND DISCUSSION

As explained last chapter, results are given under two titles regard to two main part of this study.

6.1 Electrochemical Deposition of Brushite on 316L SS and Its Conversion to Hydroxyapatite by NaOH Treatment

In this part of study, the deposition process was carried out in electrolyte no.1 under constant current densities -0.5, -5 and -10 mA/cm^2 at room temperature. For all deposition processes the total charge passed through out cell was maintained at 1800 mC (Table 5.3). Deposited coatings were immersed in 1 molar NaOH solution at 90ºC for 2 hours, where the pH of the solution was 13.5 for transformation of deposited phase by alkaline treatment.

6.1.1 Chemical Characterization by XRD, FTIR and EDS

Figure 6.1.a shows the XRD pattern of the coatings deposited under -0.5, -5, -10 mA/cm^2 and Figure 6.1.b shows the patterns of samples after NaOH treatment. The peaks at 2 theta values, 43.54º, 50.857 and 74.787 are due to the 316L stainless steel substrate (JCPDS 33-397). It is clearly seen the peaks from substrate. When the current density increased to -10mA/cm^2, aggressive gas evolution was observed on the metal surface. This can be the reason of why the peaks generating from the substrate. It also can be seen in Figure 6.1.a, main peaks of DCPD at 2 theta values, 11.579, 20.931 and 29.237 decreases with increasing current density (JCPDS 72-1240). Figure 6.1.b indicates main peaks of HA at 2 theta values, 25.827, 31.713, 32.208 and 32.923 (JCPDS 9-432) after NaOH treatment. There are also peaks from 316L substrate; it is clearly be seen main peak of 316L at 2 theta, 43.54º, increase in its intensity with increasing current density after NaOH treatment. Electrolyte wasn't aerated with $Ar_{(g)}$ or $N_{2(g)}$ during deposition process.

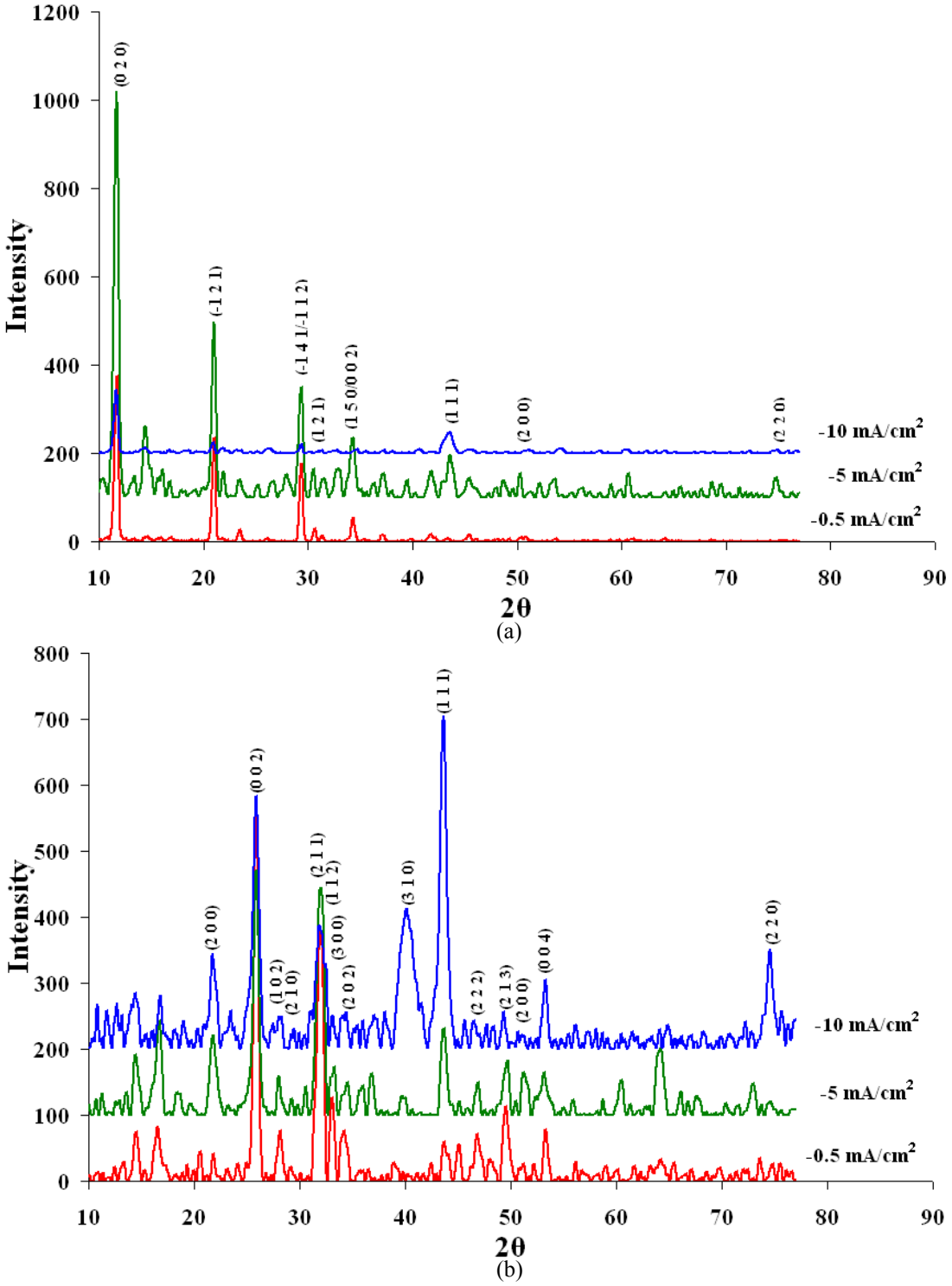

Figure 6.1 XRD patterns of coatings produced at -0.5, -5 and -10 mA/cm^2 (a) after electrochemical deposition (b) after NaOH treatment.

Table 6.1 presents the XRD peak positions of the JCPDS standard and the electrochemical depositions. The peaks of both types of electrochemical coatings matched with the standard within the expectations of experimental error.

Table 6.1 Matching 2θ values of XRD peak positions of the JCPDS standard and the electrochemical depositions (a) After deposition (b) After NaOH treatment.

(a)

Crystallographic Planes (h k l)	Standard Diffraction Peaks[a,b] (2θ)	-0.5 mA/cm^2	-5 mA/cm^2	-10 mA/cm^2
Brushite [a]72-1240 JCPDS number				
(020)	11.634	11.744	11.689	11.634
$(\bar{1}41)/(\bar{1}12)$	29.237	29.402	29.402	29.347
$(\bar{1}21)$	20.986	21.041	21.041	20.931
(121)	30.502	30.668	29.402	30.888
(150)/(022)	34.188	34.398	34.243	34.463
Austenite [b]33-397 JCPDS number				
(111)	43.650	43.375	43.650	43.540
(200)	50.802	50.857	50.362	51.077
(220)	74.732	74.842	74.787	74.897

(b)

Crystallographic Planes (h k l)	Standard Diffraction Peaks[b,c] (2θ)	-0.5 mA/cm^2	-5 mA/cm^2	-10 mA/cm^2
Hydroxyapatite [c]9-432 JCPDS number				
(211)	31.768	31.933	31.933	31.878
(300)	32.923	33.088	33.253	33.088
(112)	32.153	32.043	32.153	32.098
(002)	25.827	25.937	25.937	25.882
(202)	34.023	34.188	34.463	34.078
(102)	28.137	28.137	28.027	28.082
Austenite [b]33-397 JCPDS number				
(111)	43.650	43.705	432.650	43.650
(200)	50.802	50.857	51.187	50.692
(220)	74.732	74.787	74.621	74.566

FTIR spectra of the coatings scanned by thin film apparatus of FTIR spectrometer after galvanostatic deposition under -0.5, -5 and -10mA/cm^2 and NaOH treatment are shown in Figure 6.2.

As shown in Figure 6.2.a the presence of OH stretching (2500-3600 cm^{-1}) and H_2O bending (1645 cm^{-1}) bands are due to crystal water in DCPD, $CaHPO_4 \cdot 2H_2O$ (Fowler et al. 1966) The bands in the 1120 to 970 cm^{-1} region are described as PO_4^{3-} and HPO_4^- stretching modes (Jing et al., 2002; Mukesh et al., 1999). The band at ~865 cm^{-1} may be attributed to HPO_4^- or carbonate (CO_3^{2-}) groups since both have absorption bands close to 870 cm^{-1} (Termine & Lundy, 1973). But depending on

XRD results, the band at 865 cm^{-1} may be associated with HPO_4^{2-} ions in DCPD (Arends et al., 1987). The absorption band due to PO bending was at 561 cm^{-1} (Stulajterova & Medvecky, 2008).

In Figure 6.2.b, the strong absorbance bands at 1120-1000, 960, 600, 560 cm^{-1} are characteristic for the presence of PO_4^{3-} ions in HA, $Ca_{10}(PO_4)_6(OH)_2$ (Brown, 1966; Rey et al., 1990). The two peaks at 600 and 560 are the two well defined PO bending peaks in HA (Pleshko et al., 1991). A weak band at 3565 cm^{-1} is the characteristic of lattice OH groups in HA and it's assigned as the O-H vibration mode (Jae-Kil et al., 2006). It can also be seen in Figure 6.2.b, further decrease in the intensity of the broad band at 3500-3000 cm^{-1} and disappearance of the peak at 1645 cm^{-1} with respect to the Figure 6.2.a indicates that transformation of DCPD to HA took place after NaOH treatment. CO_3^{2-} peak present at 1408 cm^{-1} as well as the weak absorbance band at 868 cm^{-1} should arise primarily from carbonate which may be incorporated into the coatings from atmospheric CO_2 (Termine & Lundy, 1973). It's reported that carbonate content in the bone mineral is about 4-8wt. % (Burnell et al., 1980; Renugopalakrishnan et al., 1991).

The band at 960 cm^{-1} was attributed as a useful index of crystallinity in HA (Pleshko et al., 1991). In Figure 6.2.b, when the peak intensity at 960 cm^{-1} was compared with the peak intensity the peak intensity at 1012 cm^{-1}, it was found out that peak intensity at 960 cm^{-1} with respect to peak intensity at 1012 cm^{-1} increases as the current density decreases such that the most intense 960 cm^{-1} band gave rise to the most HA phase weight percent (83.3%) at the least current density, -0.5mA/cm^2 (Table 6.2). These results are also in good agreement with the given crystallinity degrees of the coatings in table 6.6.

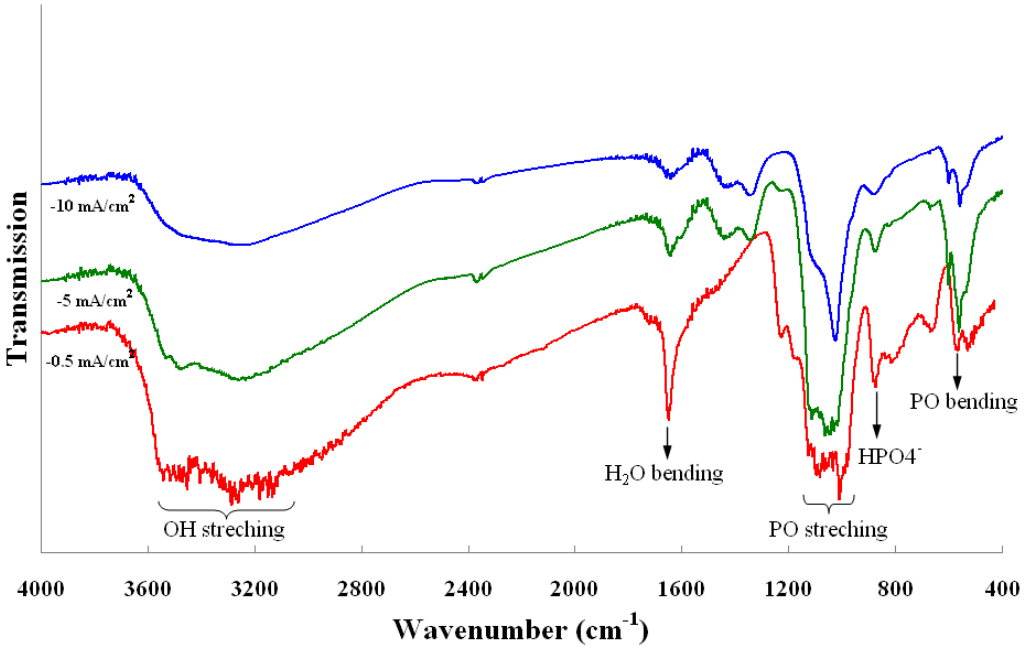

(a)

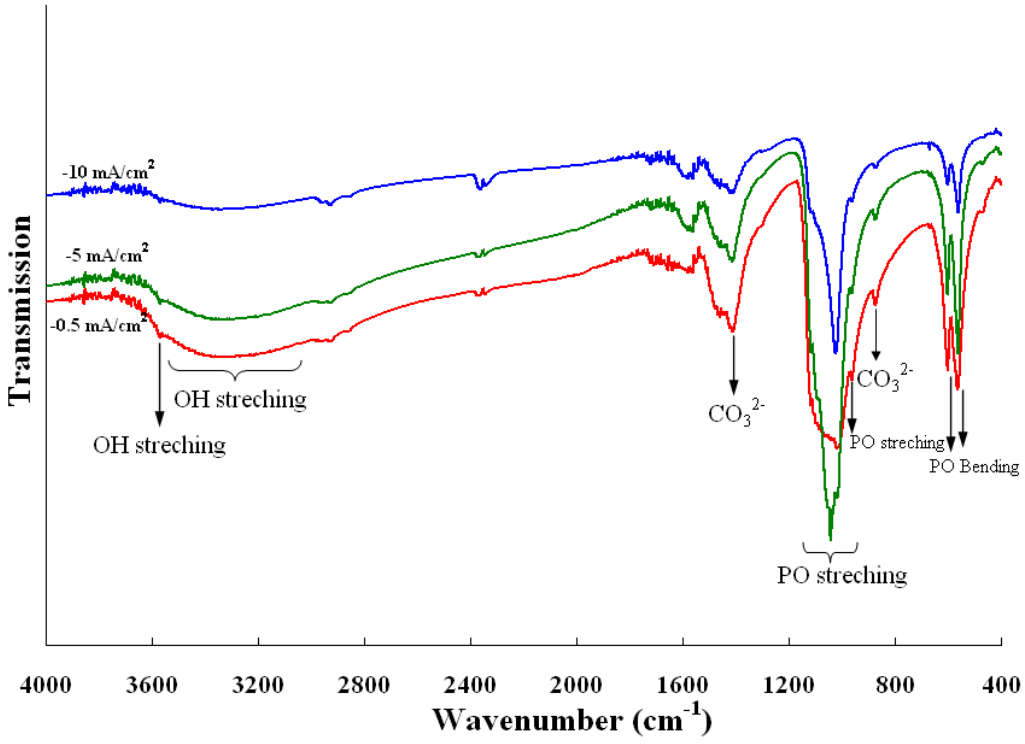

(b)

Figure 6.2 FTIR spectra of the coatings (a) after electrochemical deposition (b) after NaOH treatment.

Table 6.2 shows the quantitative analysis of crystalline components in the XRD patterns and EDS results. EDS results and quantitative analysis of crystalline components in the XRD patterns supported non-homogenous coating formed at high

current densities theory because elements of substrate give more diffractions and elements of coatings give less diffractions as the current density increases (Table 6.2). Ca/P atom ratio of the coatings after deposition was approximately 1. This result is in good agreement with XRD and FTIR results. There is also an increase in Ca/P ratio after NaOH treatment as expected. As the current density increases % wt of 316L substrate phase increases. Table 6.2 also indicates dissolution of calcium phosphate coating after NaOH treatment. Same samples were showed more % wt of austenite phase after NaOH treatment.

Table 6.2 The quantitative analysis of crystalline components in the XRD patterns and Ca/P ratios depending on EDS results.

Sample	EDS		XRD		
	Ca/P Weight Ratio	Ca/P Atom Ratio	Brushite Phase (% weight)	HA Phase (% weight)	Austenite Phase (% weight)
After Electrochemical Deposition					
-0.5 mA/cm^2	1.328	1.03	96.6	01.5	01.9
-5 mA/cm^2	1.417	1.09	78.3	05.4	16.3
-10 mA/cm^2	1.392	1.07	57.2	03.3	39.5
After NaOH Treatment					
-0.5 mA/cm^2	2.034	1.57	01.9	83.3	14.8
-5 mA/cm^2	1.924	1.49	01.7	67.6	30.7
-10 mA/cm^2	1.739	1.34	04.9	24.5	70.5

Coating/substrate weight ratio was calculated by the formula; (Ca+P)/(Fe+Cr+Ni) using the values of % wt. distribution of elements after EDS analyses. Figure 6.3 shows the coating/substrate weight ratio decreases as the current density increases as a result of decrease in coating thickness. It also can be concluded from Figure 6.3 that % weight loss of Ca and P in the coating after NaOH treatment.

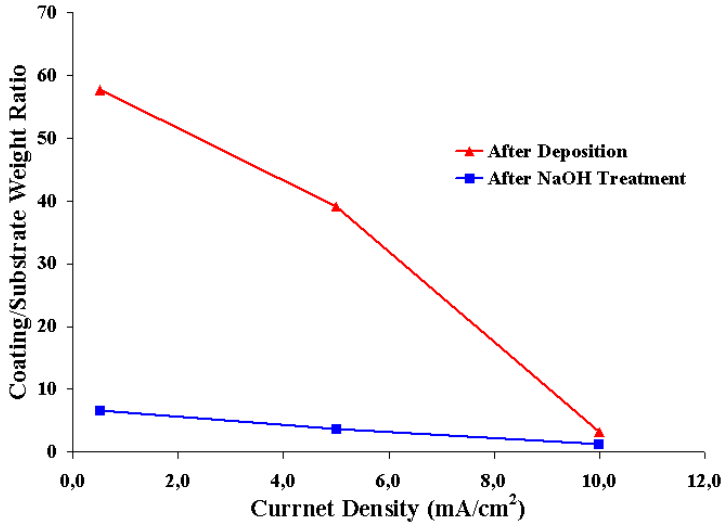

Figure 6.3 Coating / Substrate % Weight ratio [(Ca+P)/(Fe+Cr+Ni)] values calculated from EDS results.

6.1.2 Morphological Analysis by SEM

Scanning electron micrographs of the coatings produced under -0.5, -5 and -10 mA/cm^2 are shown in Figure 6.4. The coarse plate-like crystals were formed at low current density, 0.5mA/cm^2. As the current density increases, crystals size decreases. Nano sized crystals were formed at high current densities, -5 and -10 mA/cm^2. As the current density increases, electrostatic force on the crystals force them keep cluster and they seem like agglomerated locally and more compact respect to crystals formed at -0.5 mA/cm^2. As shown in Figure 6.4, coarse plate-like crystals weren't formed as the current density increased at the same charge value. Figure 6.4 (e) and (f) shows the non-homogenous coating due to -10 mA/cm^2 high current density.

The SEM images of the coatings at greater magnification are given in Figure 6.5. Two types of crystals were formed at -0.5 mA/cm ^{2} (Figure 6.5.a). Plate-like crystals and among these plates sponge like nano-sized needle like crystals are seen in Figure 6.5.b. Crystals formed at -5 mA/cm^2 are nano-sized needle like crystals (Figure 6.5.c). There is no coarse plate like crystal formation occurred. As the current density reaches -10 mA/cm^2, high electrostatic force increases the ion deposition speed and ions don't have enough time to deposit into regular crystal structures, they seem like compact and agglomerated structures as shown in Figure 6.5.c.

(a)

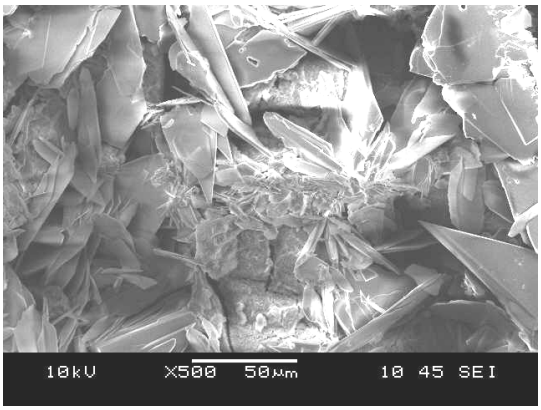

(b)

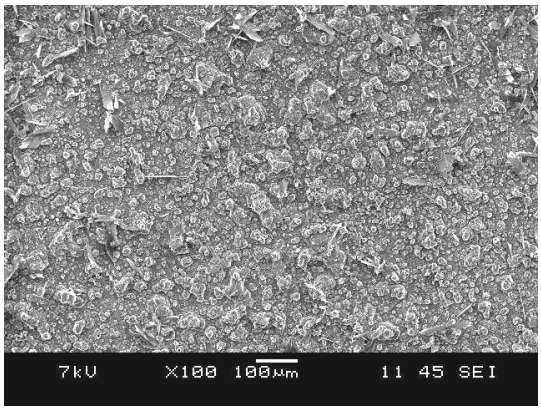

(c)

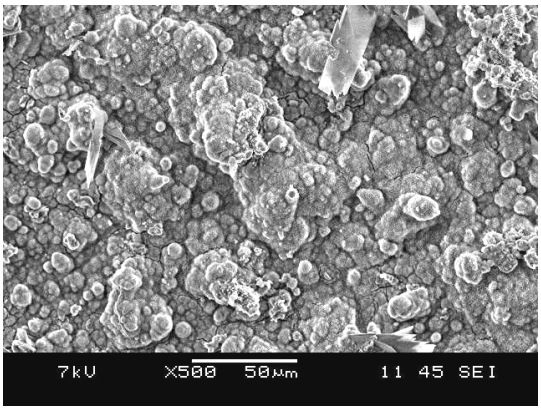

(d)

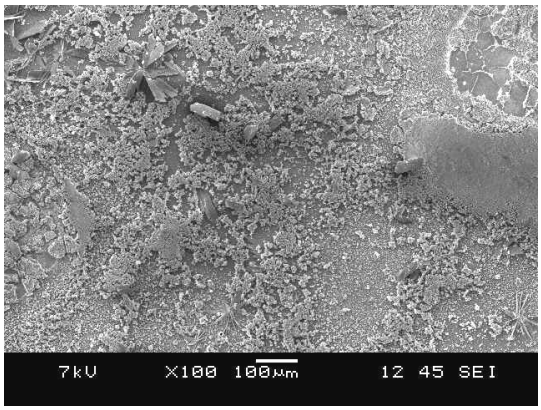

(e)

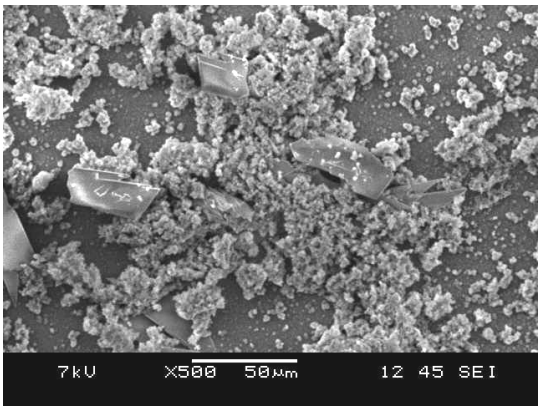

(f)

Figure 6.4 SEM images of the coatings after electrochemical deposition (a,b) -0.5 mA/cm^2 (c,d) -5 mA/cm^2 (e,f) -10 mA/cm^2.

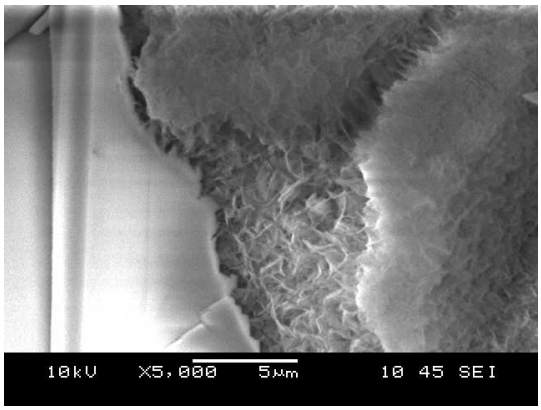

(a)

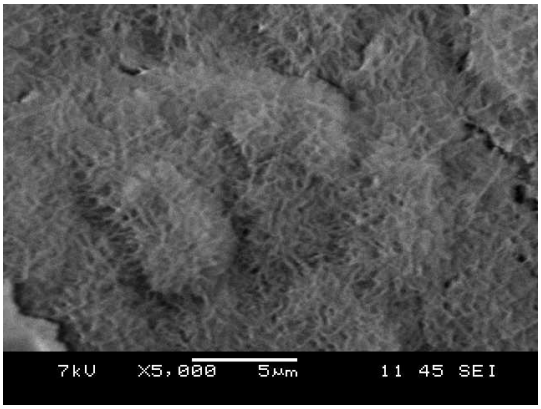

(b)

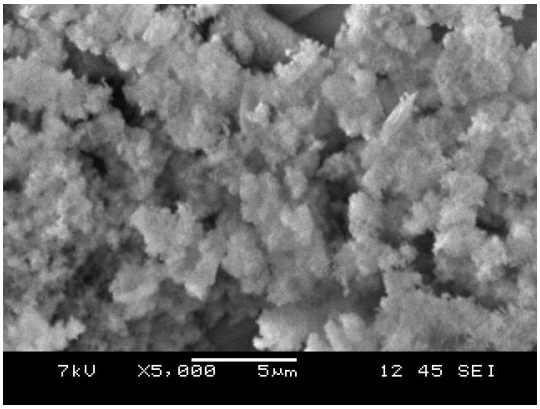

(c)

Figure 6.5 SEM images of the coatings at greater magnification after electrochemical deposition (a) -0.5 mA/cm^2 (b) -5 mA/cm^2 (c) -10 mA/cm^2.

Figure 6.6 shows the SEM images of the coatings after NaOH treatment. There are no morphological changes observed after NaOH treatment.

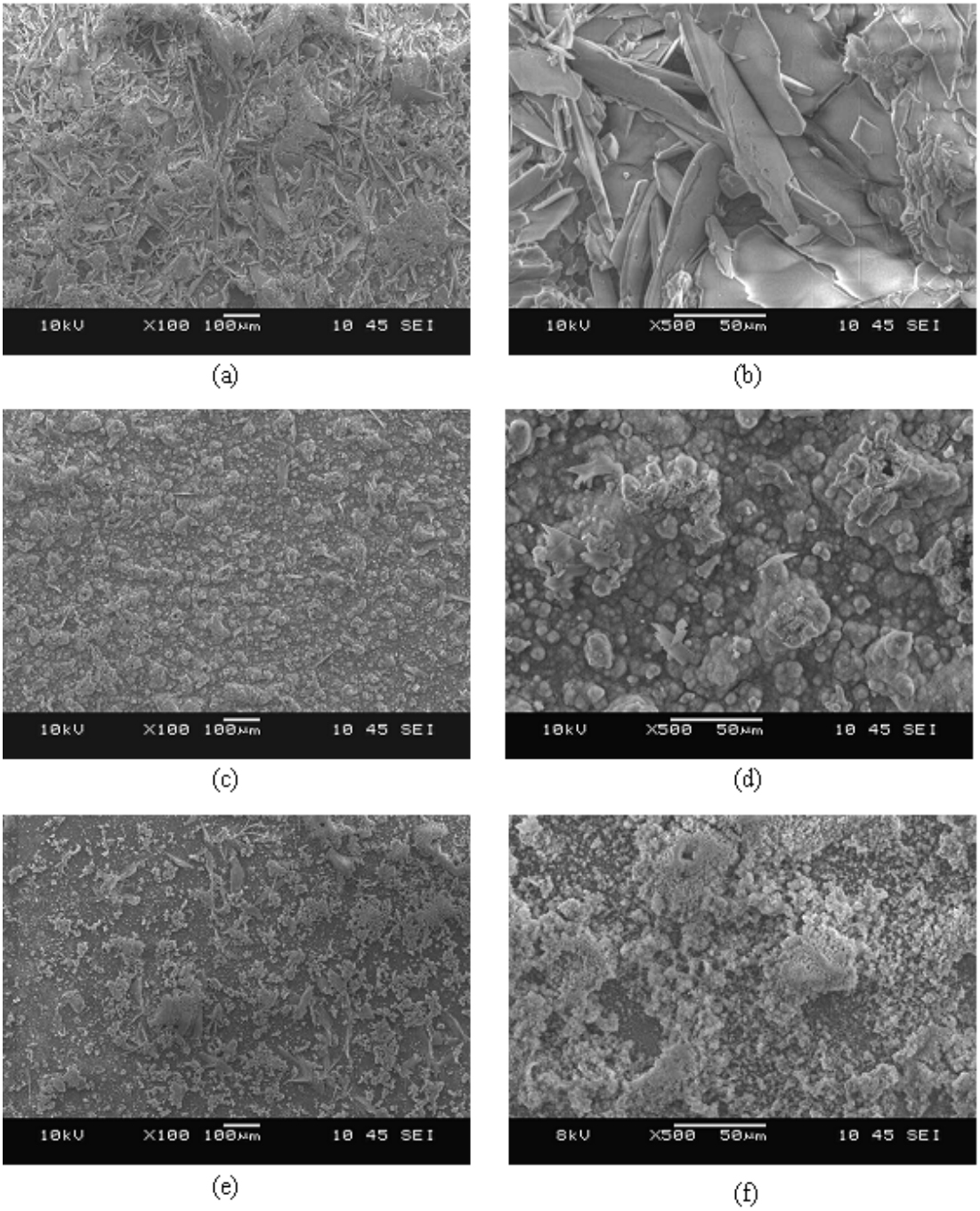

Figure 6.6 SEM images of the coatings after electrochemical deposition (a,b) -0.5 mA/cm^2 (c,d) -5 mA/cm^2 (e,f) -10 mA/cm^2.

6.2 Electrochemical Deposition of Hydroxyapatite on 316L SS

First part of the study showed that DCPD coatings were obtained by electrochemical deposition at 25 ºC in electrolyte no.1. It is known that precipitation of CaP compounds increases with increasing temperature (William, 1999). Electrolyte no.1 was highly saturated at room temperature with Ca^{2+} and PO_4^{3-} ions so it began to precipitate after 70ºC and electrolyte got muddy which is not suitable for electrodeposition of a homogenous coating. To overcome this problem electrolyte no.1 is diluted as shown in the Table 5.2 to increase the deposition temperature in order to obtain a homogenous coating. In this part of the study, electrochemical deposition was carried out controlling the 3 electrode cell system (see Figure 5.3) at different current densities -0.5, -1 and -2.5 mA/cm^2 in galvanostatic mode. Deposition temperature was adjusted to 90°C and electrolyte wasn't stirred.

6.2.1 Chemical Characterization by XRD and EDS

XRD pattern of the coatings obtained from electrolyte no.2 and no.3 are shown in Figure 6.7. The patterns show sharper peaks as the current density increases. The strongest lines in this XRD pattern corresponds to reflections at (0 0 2), (2 1 1), (1 1 2), (3 0 0), (2 0 2) planes of HA after indexing with the JCPDS file no.9-432. There are also austenite phase peaks from the substrate centered at $2\theta \approx 43.6$ and 50.8 losing their sharpness as the current density increases respect to the increase in coating thickness.

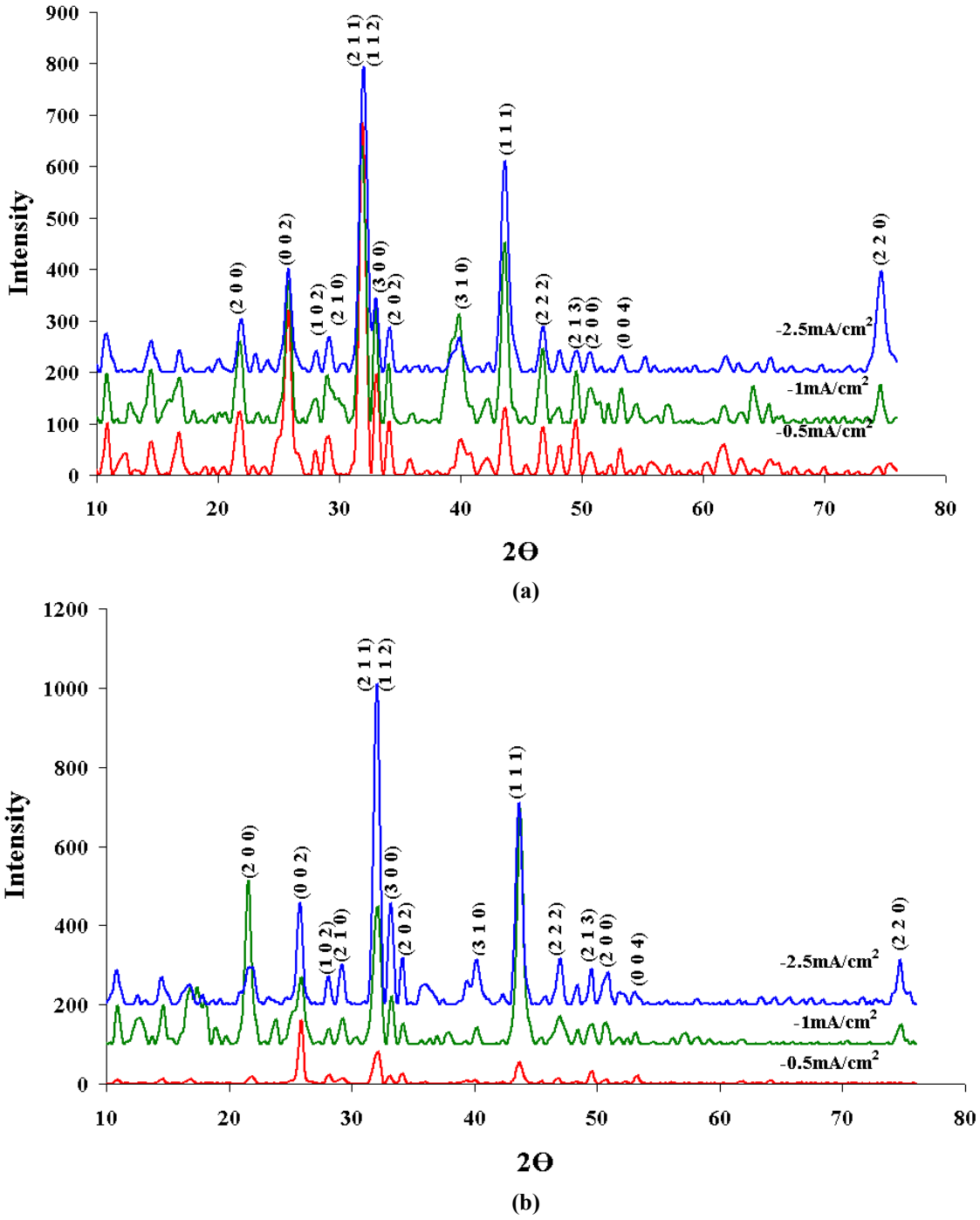

Figure 6.7 XRD patterns of HA coatings produced under various current densities in (a) electrolyte no.2 and (b) no.3.

Table 6.3 presents the XRD peak positions of the JCPDS standard and the electrochemical depositions. The peaks of both types of electrochemical coatings matched with the standard within the expectations of experimental error.

Table 6.3 Matching 2θ values of XRD peak positions of the JCPDS standard and the electrochemical depositions.

Crystallographic Planes (h k l)	Standard Diffraction Peaks[b,c] (2θ)	Location of Peaks in Deposition In Electrolyte No.3 (2θ)	Location of Peaks in Deposition In Electrolyte No.2 (2θ)
Hydroxyapatite [c]9-432 JCPDS number			
(002)	25.827	25.827	25.827
(102)	28.137	28.137	28.137
(211)	31.768	31.988	31.768
(112)	32.153	32.208	32.098
(300)	32.923	33.143	33.033
(202)	34.023	34.133	34.133
Austenite [b]33-397 JCPDS number			
(111)	43.650	43.595	43.705
(200)	50.802	50.952	50.802
(220)	74.732	74.732	74.732

Summary of quantitative analysis of crystalline components in the XRD patterns and results of EDS analysis are given in Table 6.4 to explain the effect of electrolyte concentration and current density on chemical composition of the coatings. Quantitative analysis was made by using XPowder: A software package for powder X-Ray diffraction analysis (Martin, 2004). From Table 6.4 it can be concluded that as the current density increases both Ca/P weight and atom ratio increases. Reason for this increment should be decreasing ACP amorphous phase due to increasing crystallinity. From the table, as the current density increases, % wt. of austenite phase decreases due to increase in the coating thickness according to Faraday's law.

Table 6.4 Comparison of EDS and XRD results.

Sample	EDS		XRD	
	Ca/P Weight Ratio	Ca/P Atom Ratio	HA Phase (% weight)	Austenite Phase (% weight)
Electrolyte No.2				
-0.5 mA/cm^2	1.838	1.419	52.9	47.1
-1 mA/cm^2	1.836	1.418	56.4	43.6
-2.5 mA/cm^2	1.918	1.482	80.1	19.9
Electrolyte No.3				
-0.5 mA/cm^2	1.625	1.256	29.3	70.7
-1 mA/cm^2	1.633	1.262	51.6	48.4
-2.5 mA/cm^2	1.978	1.529	52.8	47.2

In Figure 6.8 based on the EDS results, coating/substrate weight ratio versus current density is given to show increasing coating thickness in both solutions.

Coating/substrate weight ratio was calculated by the formula; (Ca+P)/(Fe+Cr+Ni) using the values of % wt. distribution of elements. From here it is also be stated that as the total charge passed through out deposition process increases, coating thickness increases.

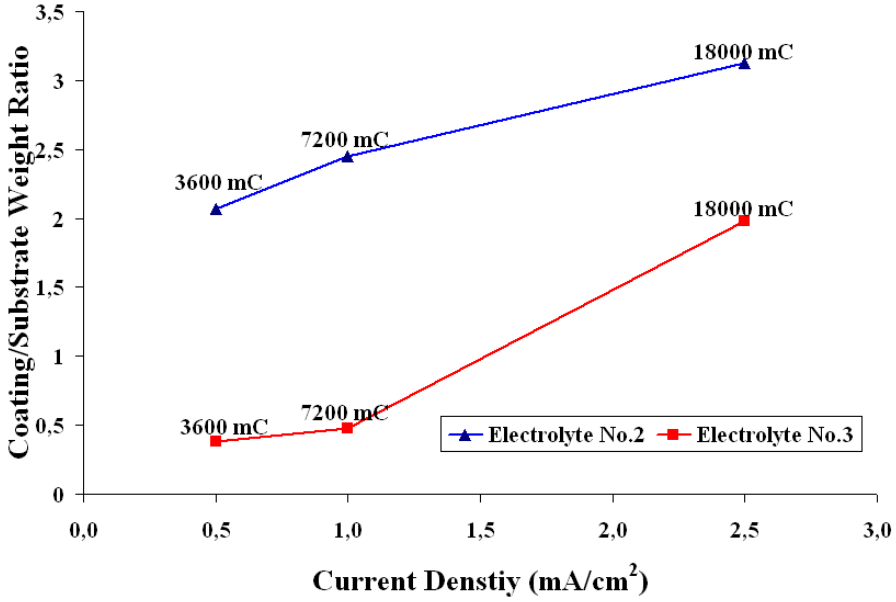

Figure 6.8 Coating/Substrate weight ratio versus current density graphic showing increasing coating thickness with increasing total charge pass through out the cell.

6.2.2 Morphological Analysis by SEM

Figure 6.9 (a-f) presents the SEM images of the coatings obtained in two electrolytes, no.2 and no.3, under -0.5mA/cm^2, -1mA/cm^2 and -2.5mA/cm^2 current density values. It is clear from the images that as the electrolyte is diluted the crystal size and morphologies of the coating changed. Different than what was observed in electrolyte no.1, the coating is composed of sphere like structures. Rößler et al. (2003) considered these spherical structures of homogenous CaP pre-layer which is reported to be amorphous calcium phosphate (ACP).

Current density is important parameter for the formation and growth of HA crystals produced in electrolytes no.2 and no.3. Nano-sized HA crystals can only be seen in the coatings formed at -0.5mA/cm^2 in the both electrolytes. These crystals were nucleated on the spherical ACP structures based on theory of Rößler et al.

(2003) and growth in a non-oriented way as can be seen in Figure 6.9 (a), (b) and Figure 6.10. As the current density increases from -0.5mA/cm^2 to -1 mA/cm^2 and -2.5 mA/cm^2, morphology of the coatings changed. Their morphology looks more compact and denser respect to morphology of the coatings formed at -0.5 mA/cm^2. As the current density increases crystal size decreases and the affect of electrical field on the crystals force them to keep closer where they agglomerated locally and formed spherical structures. This electrostatic force may increase the ion deposition speed and ions don't have enough time to deposit into regular crystal structures.

Based on the SEM results, it is shown that with decrease in ion concentration and increase in pH, the morphology of CaP coatings changes and the crystal size decreases significantly. These results clearly indicate that the ion concentrations are very important in determining nature of the CaP phases formed by electrodeposition. These results are in good agreement with Nancollas et al. (1972) and Narayanan et al. (2007), but also differ from Zhang et al. (2006) where they concluded that ion concentration has no obvious effect in changing the morphology of HA coatings.

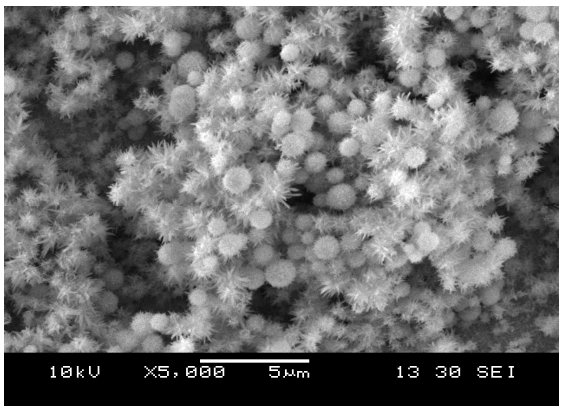

(a)

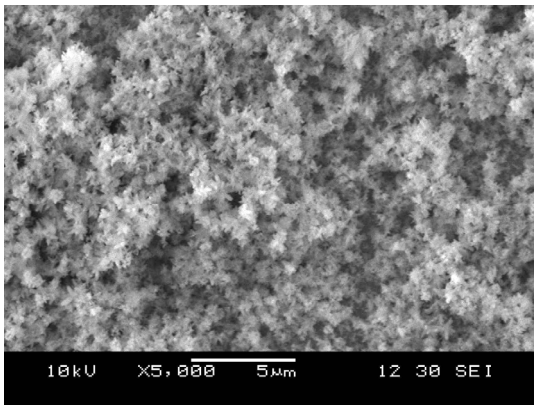

(b)

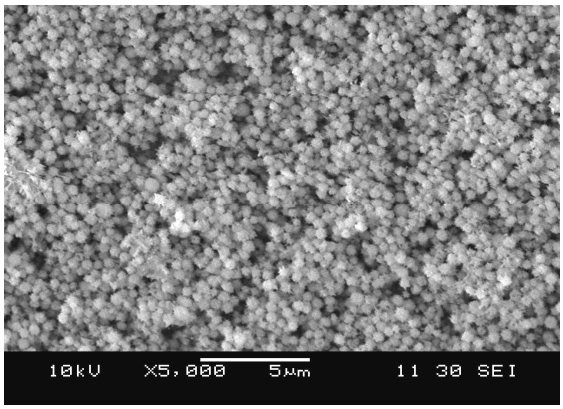

(c)

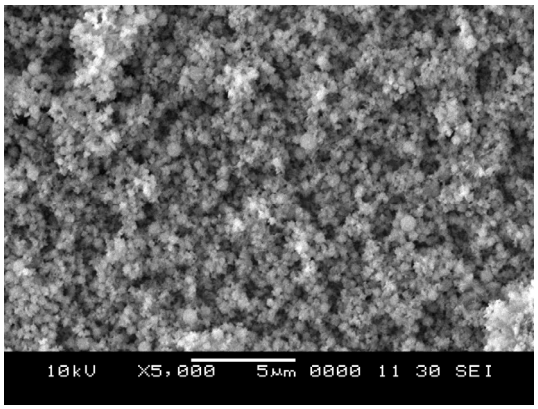

(d)

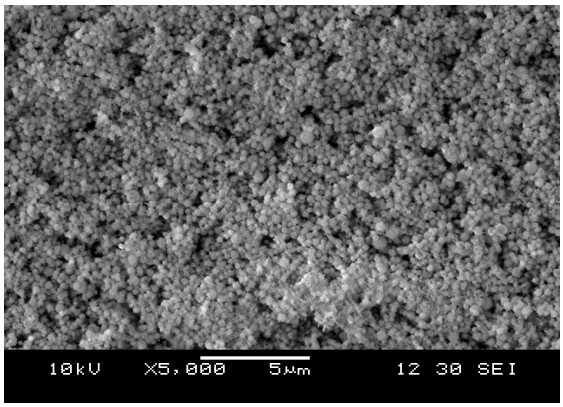

(e)

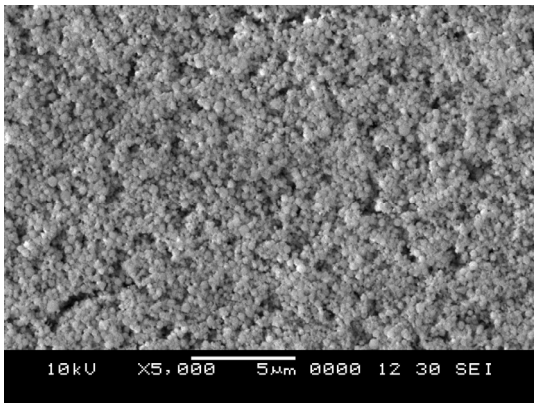

(f)

Figure 6.9 SEM images of coatings deposited in electrolytes no.2 and no.3 at various current densities for 2 hours.

(a) electrolyte no.2 / -0.5 mA/cm^2 (b) electrolyte no.3 / -0.5 mA/cm^2 (c) electrolyte no.2 / -1 mA/cm^2 (d) electrolyte no.3 / -1 mA/cm^2 (e) electrolyte no.2 / -2.5 mA/cm^2 (f) electrolyte no.3 / -2.5 mA/cm^2.

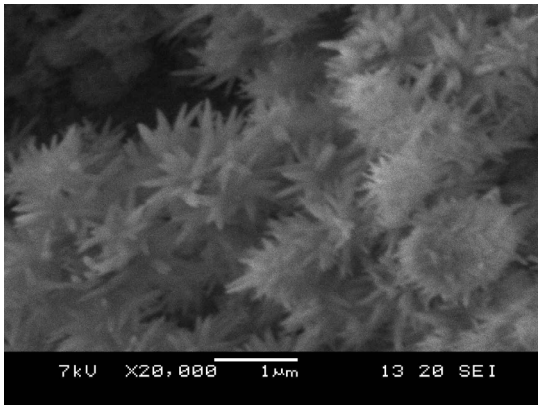

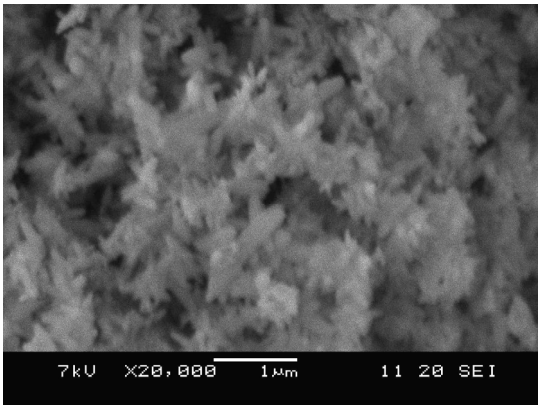

Figure 6.10 SEM images of coatings produced at -0.5 mA/cm^2 in electrolytes no.2 and no.3 showing non-oriented growth of HA crystals.

The morphological and chemical characteristics of the coatings deposited in the first and second parts of this thesis are summarized in table 6.5.

Table 6.5 The summary of electrochemical deposition parameters with deposited phases and their morphologies.

Electrolyte Number	Deposition Temperature (ºC)	Current Density (mA/cm^2)	Deposition Time (s)	Total Charge (mC)	Deposited Phase	Morphology of the coatings
No.1: 42 mM [Ca^{2+}] 25 mM [$H_2PO_4^-$] (pH=4.15)						
No.1	25	0.5	3600	1800	DCPD	Coarse plates and sponge like nano-sized crystals among the plates
No.1	25	5	360	1800	DCPD	Thin needle like nano-sized crystals
No.1	25	10	180	1800	DCPD	Agglomerated spherical like structures (more compact and denser morphology)
No.2: 2.1 mM [Ca^{2+}] 1.25 mM [$H_2PO_4^-$] (pH=5.00)						
No.2	90	0.5	7200	3600	HA	The nano-scale crystals on spherical structures
No.2	90	1	7200	7200	HA	The nano-scale crystals on spherical structures (more dense)
No.2	90	2.5	7200	18000	HA	Agglomerated spherical like structures (more compact morphology)
No.3: 1.05 mM [Ca^{2+}] 0.625 mM [$H_2PO_4^-$] (5.33)						
No.3	90	0.5	7200	3600	HA	The nano-scale crystals on spherical structures
No.3	90	1	7200	7200	HA	The nano-scale crystals on spherical structures
No.3	90	2.5	7200	18000	HA	Agglomerated spherical like structures (more compact and denser morphology)

6.3 Crystallite Size and Crystallinity Determination

6.3.1 Calculation of Crystal Size and Crystallinity

The crystallite sizes of Brushite and Hydroxyapatite was calculated by Scherrer's equation (Shih et al., 2005; Viorel et al., 2005)

$$L = \frac{0.9\lambda}{\beta_s \cos\theta}$$

Where L is the crystallite size, β_s is the full width of the peak at half of the maximum intensity (FWHM), λ denotes the wavelength of CuKα (λ=1.54178 Å) and θ is the Bragg's angle. Average crystallite size of the coatings was calculated using the most distinct reflection peaks in XRD pattern, (0 0 2) for HA and (0 2 0) for Brushite were used.

The crystallinity denoted by X_c, related to the fraction of crystalline phase in the analyzed coating. Equation 2 shows the empirical relation between X_c and the β_s:

$$\beta_s \times \sqrt[3]{X_c} = \mathrm{K_A}$$

Where X_c is the crystallinity degree, β_s is the full width of the peak at half of the maximum intensity, K_A is a constant set at 0.24 (Viorel et al., 2005)

6.3.2 Results

6.3.2.1 Crystallite Size

The average crystallite size and their corresponding crystallinity were calculated and the results are given in Table 6.6. All coatings have nano-scale crystals varied between 13 and 20 nm. It is reported that bones could heal faster with bio-ceramic coatings have nano-crystals (Ruikang et al., 2007; Yurong et al., 2004). HA crystals deposited in this thesis are in nano-scale which is suitable for osteointegration of

bone and implant surface. The results show that as the current density increases, crystallite size decreases. This indicates that crystal size can be controlled by varying the current density.

It can be also seen in Table 6.6, decrease in crystallite size after NaOH treatment. Shih et al. (2005) and Silva et al. (2001) were achieved the similar results after NaOH treatments. Results in Table 6.6 and Table 6.2 are also in good agreement with small dissolution of CaP coating after NaOH treatment occurred.

6.3.2.2 The Crystallinity

The crystallinity degree of the coatings also decreases as the current density increases (Table 6.6). This result shows that ions weren't located into regular crystal structures due to high current density and high ion deposition speed.

As explained before, index of crystallinity in hydroxyapatite was highest in the NaOH treated coating deposited at -0.5 mA/cm^2 in electrolyte No.1. These two results are also in good agreement with Table 6.2 which shows highest HA phase weight percent at -0.5 mA/cm^2 after NaOH treatment. Shih et al. (2005) observed better crystallization in 2.5M NaOH solution at 60ºC for 1 hour.

The coatings deposited at -0.5 mA/cm^2 has the highest crystallinity degree among the coatings deposited at other current densities in the same electrolyte (Table 6.6). This result shows that current density applied in electrochemical deposition of CaP coatings is the important parameter that influences the crystallinity of the coatings. Low current densities are useful for depositing coating with high crystallinity.

Table 6.6 Average crystallite size and their corresponding crystallinity degree of the coatings.

Current Density (mA/cm^2)	Electrolyte Number	Deposition Temperature (°C)	Phase	2θ values at maximum intensity (°)	FWHM (°)	Average crystal size (nm)	Crystallinity (X_c)
1st Part							
After deposition							
-0.5	No.1	25	DCPD	11.749	0.442	20	0.160
-5	No.1	25	DCPD	11.688	0.524	17	0.096
-10	No.1	25	DCPD	11.685	0.630	15	0.055
After NaOH treatment							
-0.5	No.1	…	HA	25.882	0.575	17	0.073
-5	No.1	…	HA	25.882	0.700	15	0.040
-10	No.1	…	HA	25.882	0.821	13	0.025
2nd Part							
-0.5	No.2	90	HA	25.859	0.590	15	0.067
-1	No.2	90	HA	25.859	0.785	14	0.028
-2.5	No.2	90	HA	25.793	0.864	14	0.021
-0.5	No.3	90	HA	25.876	0.452	20	0.149
-1	No.3	90	HA	25.768	0.541	17	0.087
-2.5	No.3	90	HA	25.882	0.575	17	0.073

6.4 Formation Mechanism of the Calcium Phosphate Phases

Deposition is thought to occur as a result of electrically induced pH gradient near the metal surface as described before by Shirkhanzadeh (1998). Zhang et al (1998) reported that current density is directly related to the local pH at the metal surface/electrolyte interface using in situ pH measurement technique. Besides controlling the pH, current density also controls the kinetics of the crystal growth and the morphology of the CaP coatings. Wang et al concluded that current density is the main parameter for determining the chemical properties of the crystals and which phase will be formed (Szu-Hao et al., 2005).

Redepenning et al. (1998) converted DCPD to HA by NaOH treatment. Conversion was made by using 0.1M $NaOH_{(aq)}$ solution at 95-100ºC for 18-24 hours

and at room temperature for 72 hours. Redepenning et al. also found that the conversions are effected with little overall change in the dimensions of the crystals.

Yong Han et al. (1999) succeeded in conversion of DCPD to HA by hydrothermal treatment. Conversion was made in an autoclave in the pH adjusted water with ammonia. Yong Han et al. reported Ca/P atomic ratio, grain size and pore size of HA in the coatings increase with increasing treatment temperature.

In Silva et al.'s study (2001), alkaline treatment on monotite ($CaHPO_4$) coating was made by using 0.1 M NaOH solution at 60 ºC for 1, 4, 8, 24 and 48 hours. Results showed that treatment for 4 hours was sufficient to completely transform to monotite to HA. What isn't observed in our study, they observed that after treatment for 48 hours, morphology of the coating changed significantly. As the treatment time increases, crystals appear to be fragmented at their extremities where further dissolution - reprecipitation may be occurring. They also revealed that continuous dissolution of monotite occurs at the monotite/solution interface. They succeeded in transforming monotite to HA in KOH and NH_4OH solutions at the same pH with 0.1M NaOH so transformation was irrespective of the cation present in the alkaline solution. They achieved the same results in KOH and NH_4OH solutions at the same pH with the 0.1M NaOH solution pH.

Shih et al. (2005) were investigated the affect of concentration and temperature on transformation of DCPD to HA. Treatments were done in 0.1 to 10M NaOH solutions at 30, 45, 60 and 75 ºC for 1 hour. They concluded that treatment in the 1 - 2,5M NaOH solution at a temperature higher than 60 ºC offers more proper environment for completely transformation DCPD to HA. They also revealed that increase in NaOH concentration, shorter the time taken for conversion and low treatment temperature also reduces the conversion.

It's reported that DCPD is not a stable calcium phosphate phase above pH 5.0 (Redepenning et al., 1998; Silva et al., 2001). Above this pH, it's converted to HA and this is why, pre-cursors phases; TCP (Eanes & Posner, 1968) OCP (Newesley,

1961) and DCPD (Francis & Webb, 1971) are converted to HA in-vivo conditions. Transformation mechanism of DCPD to HA can be explained thermodynamically (Silva et al. 2001). Brown et al. (1998) investigated the thermodynamic stability diagrams of some calcium phosphate compounds. Diagrams indicate that pH ranges for stability of CaP compounds showing the ionic product of calcium and phosphate expressed as a function of pH. Johnsson & Nancollas (1992) were studied the solubility phase diagram. They showed that HA is the least soluble phase at pH values above about 4.0 depending on the diagram.

It is reported that electrochemical deposition of CaP coating consists of three steps: *(i)* electrochemical reactions, *(ii)* acid-base reactions and *(iii)* precipitation reactions (Dumelié et al., 2005; Zang et al., 2006).

(i) Electrochemical reactions;

Reduction of water and NO_3^- ions are the main electrochemical reactions that change the pH of the metal/electrolyte interface by producing OH^- ions. Other electrochemical reactions involve phosphate ions;

$$2\ H_2O + 2e^- = H_2 + 2\ OH^- \quad (5.1)$$

$$NO_3^- + H_2O + 2e^- = NO_2 + 2OH^- \quad (5.2)$$

$$H_2P0_4^- + 2e^- = 2\ HPO_4^{2-} + H_2 \quad (5.3)$$

$$HPO_4^{2-} + 2e^- = 2PO_4^{3-} + H_2 \quad (5.4)$$

(ii) Acid-base reactions;

After reactions (5.1) and (5.2) if the suitable pH level is reached, acid-base reactions involving phosphate ions and hydroxide ions occur:

$$H_2P0_4^- + OH^- = HPO_4^{2-} + H_2O \quad (5.5)$$

$$HPO_4^{2-} + OH^- = PO_4^{3-} + H_2O \quad (5.6)$$

(iii) Precipitation reactions;

If the critical supersaturation level reached for HPO_4^{2-} and PO_4^{3-} ions, they will precipitate with Ca^{2+} ions at the metal surface. The pH of the metal/electrolyte interface and ions which exceed supersaturation level determine the type of CaP compound that will be formed.

If pH value is lower, formation of HPO_4^{2-} is favored according to reaction 5.3 and when there is enough HPO_4^{2-} at the metal/ electrolyte interface precipitation of DCPD will take place as shown in reaction 5.7;

$$Ca^{2+} + HPO_4^{2-} + 2\ H_2O = CaHPO_4 \cdot 2H_2O \quad (5.7)$$

When pH increases, because of higher OH^- concentrations PO_4^{3-} ion formation is favored according to reactions (5.4) and (5.6). If ion concentration of interface has enough PO_4^{3-}, after reaching supersaturation level, precipitation of HA will occur as shown in the following reaction:

$$10Ca^{2+} + 6PO_4^{3-} + 2OH^- = Ca_{10}(PO_4)_6(OH)_2 \quad (5.8)$$

Conversion DCPD to HA be occurring to continuous dissolution and re-precipitation of DCPD crystals (Shih et al., 2005; Silva et al., 2001; Nancollas, 1992) The complete transformation is depending on the pH and temperature of the treatment solution and the time that affect dissolution and re-precipitation mechanisms. In this study, DCPD crystals weren't stable thermodynamically due to the high treatment solution pH, equal to 13.5. DCPD crystals were converted to HA crystals which is the equilibrium phase at solution pH. Conversion of DCPD to HA occurs in three steps;

Dissolution of DCPD

DCPD is unstable and dissolved in 1M NaOH solution at pH 13.5.

$$CaHPO_4 \cdot 2H_2O = Ca^{2+} + HPO_4^{2-} + 2\ H_2O \quad (5.9)$$

Acid-Base Reaction

When DCPD was dissolved, acidic HPO_4^{2-} ions reacted with OH^- ions of basic treatment solution as described in reaction (5.6).

$$HPO_4^{2-} + OH^- = PO_4^{3-} + H_2O \quad (5.6)$$

Precipitation of HA

Products of reaction (5.9) and (5.6) are Ca^{2+} and PO_4^{3-} ions react with OH- ions of treatment solution according to the reaction (5.8) to form HA which is stable phase at pH 13.5.

$$10Ca^{2+} + 6PO_4^{3-} + 2OH^- = Ca_{10}(PO_4)_6(OH)_2 \quad (5.8)$$

CHAPTER SEVEN
CONCLUSIONS

Brushite and Hydroxyapatite coatings on 316L stainless steel were prepared by galvanostatic electrochemical deposition method using electrolytes having different Ca^{2+} and $H_2PO_4^-$ ion concentrations at different temperatures. NaOH alkaline treatment was applied to DCPD coatings. Effect of current density on coating morphology and chemical composition was investigated. The following conclusions depended on experimental studies were obtained:

1. DCPD coatings on the 316L stainless steel were deposited by electrochemical deposition in electrolyte containing 42mM $Ca(NO_3)_2 \cdot 4H_2O$ and 25 mM $NH_4H_2PO_4$ (pH=4.15) at room temperature. HA phase was deposited in the electrolytes that have 2.1mM, 1.05mM $Ca(NO_3)_2 \cdot 4H_2O$ and 1.25mM, 0.625mM $NH_4H_2PO_4$ (pH=5.00 and pH=5.33) at 90 ºC.

2. Besides the electrochemical deposition parameters like current density, pH of the electrolyte is the one of the main parameters that determines which calcium phosphate phase will be deposited.

3. Crystal sizes of the coatings decreased as the current density increased. DCPD coatings were deposited in electrolyte No.1 at 25ºC showed different morphologies depending on the current density. Plate-like crystals were obtained under current density of -0.5 mA/cm^2 and nano-sized needle like crystals were formed under current density of -5 mA/cm^2. Spherical like structures were observed in the HA coatings that were deposited in electrolytes No.2 and No.3 at 90 ºC. All coatings deposited by galvanostatic electrochemical deposition have nano-scale crystals with 16 nm average crystal size.

4. The crystallinity degree of the coatings also decreased as the current density increased.

5. The current density showed no effects on the chemical composition of the coatings.

6. XRD and FTIR results showed that after NaOH treatment, transformation of DCPD to HA was achieved in 1 molar NaOH solution at 90ºC for 2 hours. EDS results were also supported XRD and FTIR results.

7. After NaOH treatment morphology of the coatings showed no significant changes except for a small amount of size reduction.

8. The CO_3^{2-} incorporation in HA coatings after NaOH treatment were observed in FTIR spectra. These result shows that 316L stainless steel surface can be coated with CO_3^{2-} incorporated HA having nano-scale crystals for improving the bone in growth and biocompatibility.

Further Study

1. It's recommend that in vivo tests can be conducted to investigate the effects of cells on chemical stability and biocompatibility properties of HA coatings.

2. To evaluate the chemical stability and dissolution properties of HA coatings in vitro tests, like corrosion and cell attachment tests, should be performed.

3. Performance of HA coatings should be improved by deposition of other calcium phosphate compounds on HA coating. These functionally graded films can improve the performance of the implant in vivo and in vitro conditions.

4. The mechanical properties of the HA coatings should be improved by reinforcement of the coating with polymer, alumina (Al_2O_3) or zirconia (ZrO_2) etc.

REFERENCES

Arends, J., Christoffersen, J., Christoffersen, R., Eckert, E., Fowler, B., Heughebaert, C., Nancollas, G., Yesinowski, J. & Zawacki, J. (1987). A calcium hydroxyapatite precipitated from an aqueous solution. *Journal of crystal growth*, 84, 515-532.

Balcik, C. (2002). *Biomechnaics of porous ceramic implants used in long bone segmental defect healing*. PhD Thesis, Middle East Technical University, Ankara, Turkey.

Ban, S., & Maruno, S. (1998). Hydrothermal-electrochemical deposition of hydroxyapatite. *Journal of Biomedical Materials Research,*42(3), 387-395.

Beevers, C.J. & Robinson, J.L. (1969). Some observations on the influence of oxygen content on the fatigue behavior of α-titanium alloy. *Journal of. Less Common Metals*, 17, 345-352.

Boneli, A. (1994). Current concepts in orthopaedic biomaterials and implant fixation. *The Journal of Bone and Joint Surgery*, 76, 1897-1898.

Brown, P., LeGeros, R.Z., & LeGeros, J.P. (Eds.). (1998). *Bioceramics 11*, World UK: Scientific Publishing Co.

Brown, W. (1966). Crystal growth of bone mineral. *Clinical Orthopedic*, 44, 205-220.

Brunski, J. B. (1996). *Metals, Biomaterials Science: An Introduction to Materials in Medicine*, London: Academic Press, 37-50.

Burnell, J. M., Teubner, E. J., & Miller, A. G. (1980). Normal maturational changes in bone matrix, mineral, and crystal size in the rat. *Calcified Tissue International,* 31, 13-19.

Coathulp, M. J., Blunn, G. W., Flynn, N., Williams, C., & Thomas, N. P. (2001). A comparison of bone remodelling around hydroxyapatite-coated, porous-coated and grit-blasted hip replacements retrieved at postmortem. *The Journal of Bone and Joint Surgery*, 83-B, 118-123.

Compte, P., Boretos J.W. & Eden M., (eds.). (1984). *Metallurgical observations of biomaterials. in Contemporary Biomaterials*, Park Ridge, NJ: Noyes Pub.

Cook, S. D., Thomas, K. A., Kay, J. F., & Jarcho, M. (1988). Hydroxyapatite-coated porous titanium for use as an orthopedic biologic attachment system. *Clinical Orthopaedics and Related Research*, 230, 303-312.

Cotell, C.M., Chrisey, D.B., & Hubler, G.K. (Eds.). (1994). *Pulsed Laser Deposition of Thin Films*, Wiley, Chichester.

Da Silva, M.H.P., Lima, J.H.C, Soares, GA, Elias C.N., de Andrade, M.C, Best, S.M., & Gibson, I.R. (2001). Transformation of monetite to hydroxyapatite in bioactive coatings on titanium. *Surface and Coatings Technology*, 137, 270.

Dalton, J. E., Cook, S. D., Thomas, K. A., & Kay, J. F. (1995). The effect of operative fit and hydroxyapatite coating on the mechanical and biological response to porous implants. *The Journal of Bone and Joint Surgery*, 77-A, 97-110.

Dasarathy, H., Riley, C., Coble, H.D., Lacefield, W.R., & Maybee, G. (1996). Hydroxyapatite/metal composite coatings formed by electrocodeposition. *Journal of Biomedical Materials Research* May, 31, 81-9.

Davis, J.R. (2004). *Handbook of Materials for Medical Devices* (2nd ed.). New York: ASTM STP, 684.

Donachie, M. (1998). *Biomaterials, Metals Handbook Desk Edition*. New York: ASM International, 702-709.

Dumelié, N., Benhayoune, H., Rousse-Bertrand, C., Bouthors, S., Perchet, A., Wortham, L., Douglade, J., Laurent-Maquin, D., & Balossier, G. (2005). Characterization of electrodeposited calcium phosphate coatings by complementary scanning electron microscopy and scanning-transmission electron microscopy associated to X-ray microanalysis. *Thin Solid Films*, 492(1-2), 131-139.

Eanes, E.D., & Posner, A.S., (1968). Intermediate phases in the basic solution preparation of alkaline earth phosphates. *Calcified Tissue Research*, 2, 38.

Eliaz, N., Sridhar, T. M., Kamachi, M., & Baldev, R. (2005). Electrochemical and electrophoretic deposition of hydroxyapatite for orthopaedic applications. *Surface Engineering*, 21, 238-242.

Fowler, B. O., Moreno, E. C., & Brown, W. E. (1966). Infra-red spectra of hydroxyapatite, octacalcium phosphate and pyrolysed octacalcium phosphate. *Archives of Oral Biology*, 11(5), 477-492.

Francis, M.D., & Webb, N.C. (1971). Hydroxyapatite formation from a hydrated calcium mono-hydrogen phosphate precursor. *Calcified Tissue Research*, 6, 335.

Fu, Y., Batchelor, A.W. & Khor, K.A. (1999). Fretting wear behavior of thermal sprayed hydroxyapatite coating lubricated with bovine albumin, *Wear*, (230), 98-102.

Granchi, D., Ciapetti, G., Stea, S., Savarino, L., Filippini, F., Sudanse, A, Zinghi, G., & Montanaro, L. (1999). Cytokine release in mononuclear cells of patients with Co-Cr hip prosthesis. *Biomaterials*, 20, 1079-1086.

Gronowicz, G., & McCarthy, M. B. (1996). Response of human osteoblasts to implant materials: integrin-mediated adhesion. *Journal of Orthopaedic Research*, 14, 878-887.

Gurmeric¸ A. (1995). *Experimental evaluation of new bone formation using hydroxyapatite, allogenic bone chips, natural coral and calcium carbonate*. PhD Thesis, Hacettepe University, Ankara, Turkey.

Haddow, D.B., James, P.F., & Van Noort, R. (1996). Characterization of sol-gel surfaces for biomedical applications. *Journal of Materials Science: Materials in Medicine*, 7, 255–260.

Hamdi, M., Hakamata, S., & Ektessabi, A.M., (2000). Coating of hydroxyapatite thin film by simultaneous vapor deposition. *Thin Solid Films*, 377-378, 484.

Head, W. C., Bauk, D. J., & Emerson, R. H. (1995). Titanium as the material of choice for cementless femoral components in total hip arthroplasty. *Clinical Orthopaedics and Related Research*, 311, 85-90.

Hench, L.L. (1985). *Inorganic biomaterials: In Advances in chemistry. No: 245. Materials chemistry - an emerging discipline*. Washington DC: American Chemical Society, 523.

Hench, L.L. (1991). Bioceramics: From Concept to Clinic. *Journal of the American Ceramic Society*, 74, 1487-1510.

Hofmann, A.A., Bloebaum, R.D., & Bachus, K.N. (1997). Progression of human bone ingrowth into porous-coated implants. *Acta Orthopaedica Scandinavica*, 68, 161-166.

Hu., H.B., Lin, C.J., Hu, R., & Leng, Y.A. (2002). Study on hybrid bioceramic coatings of HA'poly (vinyl acetate) co-deposited electrochemically on Ti-6A14V alloy surface. *Materials Science & Engineering C,* 20(1-2), 209-214.

Hulshoff, J.E.G., van Dijk, K., van der Waerden, J.P.C.M, Wolke, J.G.C, Ginsel, L.A, & Jansen, J.A. (1995). Biological evaluation of the effect of magnetron sputtered Ca/P coatings on osteoblast-like cells in vitro. *Journal of Biomedical Materials Research*, 29, 967,975.

Jae-Kil, H., Ho-Yeon, S., Fumio, S., & Byong-Taek, L. (2006). Synthesis of high purity nano-sized hydroxyapatite powder by microwave-hydrothermal method. *Materials Chemistry and Physics*, 99, 235-239.

Jing, X., Riley, C., Kumar, M., & Krishnan, C. (2002). FTIR/ATR study of protein adsorption and brushite transformation to hydroxyapatite. *Biomaterials*, 23, 3609-3616.

Jinno, T., Goldberg, V. M., Davy, D., & Stevenson, S. (1998). Osseointegration of surface-blasted implants made of titanium alloy and cobalt–chromium alloy in a rabbit intramedullary model. *Journal of Biomedical Materials Research*, 42, 20-29.

Jody, R., Tom, S., Sandra, B., Louis, L., & John, M. (1998). Characterization of electrolytically prepared brushite and hydroxyapatite coatings on orthopedic alloys. *Journal of Biomedical Materials Research*, 30(3), 287-294**.**

Johnsson, M. S., & Nancollas, G. H. (1992). The Role of Brushite and Octacalcium Phosphate in Apatite Formation, *Critical Reviews in Oral Biology & Medicine*, 3, 61-82.

Johnsson, M., & Nancollas, G.H. (1992). The role of brushite and octacalcium phosphate in apatite formation. *Critical Reviews in Oral Biology & Medicine*, 3, 61-82.

Kangasniemi, I.M., Verheyen, C.C., Van der Velde, E.A., & De Groot, K. (1994). In vivo tensile testing of fluorapatite and hydroxyapatite plasma-sprayed coatings. *Journal of Biomedical Materials Research,* 28, 563-572.

Kasemo, B., & Lausmaa, J. Ratner B.D. (eds.). (1988). *Biomaterials from a surface science perspective. İn Surface Characterization of Biomaterials*, New York: Elsevier.

Kapanen, A., Kinnunen, A., Ryhanen, J., & Tuukkanen, J. (2002). TGF-beta secretion of ROS-17/2.8 cultures on NiTi implant material. *Biomaterials*, 23, 3341-3346.

Klein, T., Patka, P., Wolke, C., de Blieck-Hogervost, A., & de Groot, K. (1994). Features of calcium phosphate plasma-sprayed coatings: An in vitro study. *Journal of Biomedical Materials Research*, 28, 961-967.

Koc, N., & Timucin, M. (1999). Medical ceramics. *Arthroplasty Arthroscopic Surgery*, 10, 104-109.

Koch, C.F., Johnson, S., Kumar, D., Jelinek, M., Chrisey, D.B., Doraiswamy, A., Jin, C., Narayan, R.J., & Mihailescu, I.N. (2007). Pulsed laser deposition of hydroxyapatite thin films. *Materials Science and Engineering,* 27(3), 484-494.

Krajewski, A., Ravaglioli, A., Roncari, E., Pinasco, P., & Montanari, L. (2000). Porous ceramic bodies for drug delivery. *Journal of Materials Science: Materials in Medicine*, 12, 763-771.

Kumar, M., Xie, J., Chittur, K., & Riley, C. (1999). Transformation of modified brushite to hydroxyapatite in aqueous solution: effects of potassium substitution. *Biomaterials*, 20, 1389-1399.

Kuo, M.C., & Yen, S.K. The process of electrochemical deposited hydroxyapatite coatings on biomedical titanium at room temperature. *Materials Science & Engineering C*, 2002, 153-160.

Kweh, S.W.K., Khor, K.A. & Cheang, P. (2000). Plasma-sprayed hydroxyapatite (HA) coatings with flame-spheroidized feed stock: Microstructure and mechanical properties. *Biomaterials*, (21), 1223-1234.

Lazic, S., Zec, S., Miljevic N. & Milonjic S. (2001). The effect of temperature on the properties of hydroxyapatite precipitated from calcium hydroxide and phosphoric acid. *Thermochimica Acta*, 374, 13-22.

Leeuwenburgh, S., Wolke, J., Schoonman, J. & Jansen, J. (2003). Electrostatic spray deposition (ESD) of calcium phosphate coatings, *Journal of Biomedical Materials Research A*, 66A(2), 330-334.

Li, P., & de Groot, K.J. (1994). Better bioactive ceramics through sol-gel process. Sol-Gel Science and Technology, 2, 797– 801.

Lima, R.S., Khor, K.A., Li, H., & Marple, B.R. (2005). HVOF spraying of nanostructured hydroxyapatite for biomedical applications. *Materials Science & Engineering A*, 396, 181-187.

Liu, F., Wang, F., Shimizu, T., Kaoru, I., & Zhao, L. (2006). Hydroxyapatite formation on oxide films containing Ca and P by hydrothermal treatment. *Ceramics International*, 32(5), 527-531.

Lopez-Heredia, M. A., Weiss, P., & Layrolle, P. (2007). An electrodeposition method of calcium phosphate coatings on titanium alloy, *Journal of Materials Science: Materials in Medicine*, 18, 381-390.

Lu, Y.P., Li, M.S., Li, S.T., Wang, Z.G. & Zhu R.F. (2004). Plasma-sprayed hydroxyapatite+titania composite bond coat for hydroxyapatite coating on titanium substrate. *Biomaterials*, 25(18), 4393.

Manso, M., Jimenez, C., Morant, C., Herrero, P., & Martnez-Duart, J. (2000). Electrodeposition of hydroxyapatite coatings in basic conditions. *Biomaterials*, 21, 1755-1761.

Maquet V., Boccaccini A.R., Pravata L., Notinger I. & Jerome R.(2003). Preparation, characterization and in vitro degradation of bioresorbable and bioactive composites based on Bioglass (Trademark) filled polylactide foams, *Journal of Biomedical Materials Research, Part A*, 66A(2), 35-346.

Martin, J.D. (2004). Using XPowder: A software package for powder X-Ray diffraction analysis. www.xpowder.com. D.L. GR 1001/04.ISBN 84-609-1497-6. 105 p. Spain.

Meyer, J. L., & Nancollas, G. H. (1972). The Effect of pH and Temperature on the Crystal Growth of Hydroxyapatite. *Archives of Oral Biology*, 17, 1623.

Michael, J.Y., Debra, J.T., Kai-Uwe, L., Vasif , H., David, E.A., & Donald L.W. (2004). *Biomaterials in Orthopedics*. New York: Marcel Dekker Inc.

Midy, V., Dard, M., & Hollande, E. (2001). Evaluation of the effect of three calcium phosphate powders on osteoblast cells. *Journal of Materials Science: Materials in Medicine*, 259-265.

Milthorpe, B.K. (2000). *Hydroxyapatite based materials for replacement of bone in load bearing situations.* Proc. 10th International Conference on Biomedical Engineering, Singapore, edit. JCH Goh, publ. National University of Singapore, 6-9 Dec. 2000, Singapore, pp. 38-39.

Montanaro, L., Arciola, C.R., Campoccia, D., & Cervellati, M. (2002). In vitro effects of MG63 osteoblast-like cells following contact with two roughness-differing fluorohydroxyapatite-coated titanium alloys. *Biomaterials*, 23, 3651-3659.

Nancollas, G.H. (1992). The involvement of calcium phosphates in biological mineralization and demineralization processes. *Pure and Applied Chemistry*, 64(11), 1673-1678.

Narayanan, R., Seshadri, S. K., Kwon, T. Y. & Kim, K. H. (2007). Electrochemical nano-grained calcium phosphate coatings on Ti–6Al–4V for biomaterial applications. *Scripta Materialia*, 56(3), 229-232.

Newesley, H. (1961). Changes in crystal types of low solubility calcium phosphates in carbonated compounds of accompanying ions. *Archives of Oral Biology*, 6, 174.

Niinomi, N. (1999). Recent titanium R&D for biological applications in Japan. *Journal of the Minerals, Metals and Materials Society*, 51(6), 32-34.

Pilliar, R. M. (1990). *Porous Biomaterials. Concise Encyclopedia of Medical & Dental Materials.* USA: Permagon Press and The MIT Press, 312-319.

Pillar, R.M. & Weatherly, G.C. (1984). Developments in implant alloys. *CRC Critical Reviews in Biocompatability*, 1(4), 371-403.

Pleshko, N., Boskey, A., & Mendelsohn, R. (1991). Novel infrared spectroscopic method for the determination of crystallinity of hydroxyapatite minerals. *Biophysical Journal*, 60(4), 786-93.

Praemer, A., Furner, S., & Rice, DP. (1992). Musculoskeletal conditions in the United States, Illinois. *American Academy of Orthopaedic Surgeons*, 127-141.

Rahal, M.D., Branemark, P.I., & Osmond, D.G. (1993). Response of bone marrow to titanium implants. *International Journal of Oral & Maxillofacial Implants*, 8, 573-579.

Ratner, B.D. et al. (1996). *Biomaterials Science: An Introduction to Materials in Medicine.* USA: Academic Press.

Redepenning, J., Venkataram, G., Chen, J. & Stafford, N. (2003). Electrochemical preparation of chitosan/hydroxyapatite composite coatings on titanium surfaces, *Journal of Biomedical Materials Research A*, 66A(2), 411-416.

Rey, C., Renugopalakrishnan, V., Collins, B., & Glimcher, M. (1991). Fourier transform infrared spectroscopic study of the carbonate ions in bone mineral during aging. *Calcified Tissue International*, 49, 251-258.

Rey, C., Shimizu, M., Collins, B., & Melvin, J.G. (1990). Resolution-enhanced Fourier transform infrared spectroscopy study of the environment of phosphate ions in the early deposits of a solid phase of calcium-phosphate in bone and enamel and their evolution with age.: Investigation in the v4 PO4 domain". *Calcified Tissue International*, 46, 384-394.

Rey, C., Shimizu, M., Collins, B., Melvin, J.G. (1990). Resolution-enhanced Fourier transfom infiared spectroscopy study of the environment of phosphate ions in the early deposits of a solid phase of calcium-phosphate in bone and enamel and their evolution with age: Investigation in the v4 PO4 domain. *Calcified Tissue International*, 46, 384-394.

Rößler, S., Sewing, A., Stölzel, M., Born, R., Scharnweber, D., Dard, M., & Worch, H. (2003). Electrochemically assisted deposition of thin calcium phosphate coatings at near-physiological pH and temperature. *Journal of Biomedical Materials Research*, 64A(4), 655-663.

Ruikang, T., Lijun W., & Nancollas, H. (2004). Size-effects in the dissolution of hydroxyapatite: an understanding of biological demineralization, *Journal of Materials Chemistry*, 14, 2341-2346.

Santavirta, S., Gristina, A., & Konttinen, YT. (1992). Cemented versus cementless hip arthroplasty: a review of prosthetic biocompatibility. *Acta Orthopaedica Scandinavica*; 63: 225-232.

Savarino, L., Granchi, D., Ciapetti, G., Cenni, E., Greco, M., Rotini, R., Vernosesi, C.A., Baldini, N. & Giunti, A. (2003). Ion release in stable hip arthroplasties using metal-on-metal articulating surfaces: A comparison between short-term and long-term results. *Journal of Biomedical Materials Research A*, 66A(3), 450-456.

Savarino, L., Fini, M., Ciapetti, G., Cenni, E., Granchi, D., Baldini, N., Greco, M., Rizzi, G., Giardino, R. & Giunti, A. (2003). Biologic effects of surface roughness and fluorhydroxyapatite coating on osteointegration in external fixation systems: An *in vivo* experimental study, *Journal of Biomedical Materials Research A,* 66A(3), 652-661.

Schlesinger, M., & Paunovic, M. (2000). *Modern Electroplating* (4th ed.). New York: Wiley.

Schroeder, A., Van der Zypen, E., Stich, H. & Sutter, F. (1981). The reaction of bone, connective tissue and epithelium to endosteal implants with sprayed titanium surfaces. *International Journal of Oral and Maxillofacial Surgery,* 9, 15-25.

Seiji, B., & Shiego, M. (1998). Morphology and microstructure of electrochemically deposited calcium phosphates in a modified simulated body fluid. *Biomaterials*, 19, 1245-1253.

Shah, A. K., Sinha, R. K., Hickok, N. J., & Tuan, R. S. (1999). High-resolution morphometric analysis of human osteoblastic cell adhesion on clinically relevant orthopedic alloys, *Bone*, 24(5), 499-506.

Shanbhag, A. S., Jacobs, J. J., Glant, T. T., Gilbert, J. L., Black, J., & Galante, J. O. (1994). Composition and morphology of wear debris in failed uncemented total hip arthroplasty. *The Journal of Bone and Joint Surgery*, 76-A, 60-67.

Shih, W.J., Yi-Hung, C., Szu-Hao, W., Wang-Long, L., Min-Hsiung, H., & Moon, C.W. (2005). Effect of $NaOH_{(aq)}$ treatment on the phase transformation and morphology of calcium phosphate deposited by an electrolytic method. *Journal of Crystal Growth*, 285, 633-641.

Shinto, Y., Uchida, A., Korkusuz, F., Araki, N., & Ono, K. (1992). Calcium hydroxyapatite ceramic used as a delivery system for antibiotics. *The Journal of Bone and Joint Surgery*, 74-B, 600-604.

Shirkhanzadeh, M. (1995). Calcium phosphate coatings prepared by electrocrystallisation from aqueous electrolytes. *Journal of Material Science: Materials in Medicine*, 6, 90-93.

Shirkhanzadeh, M. (1998). Direct Formation of nanophase hydroxyapatite on cathodically polarized electrodes. *Journal of Material Science: Materials in Medicine*, 9, 67-72.

Siegel, R.W., Ramasamy, S., Hahn, H., Li, Z., Lu, T. & Gronsky, R. (1998). Synthesis, characterization, and properties of nanophase TiO_2. *Journal of materials research,* 3, 1367.

Smith, T. (1994). The Effect of Plasma-Sprayed Coatings on the Fatigue of Titanium Alloy Implants. *Journal of the Minerals, Metals and Materials Society*, 54-56.

Sovak, G., Weiss, A., & Gotman, I. (2000). Osseointegration of Ti6Al4V alloy implants coated with titanium nitride by a new method. *The Journal of Bone and Joint Surgery*, 82-B, 290-296.

Sridhar, T. M., Arumugan, T. K., & Rajeswari, M. (1997). Electrochemical behaviour of hydroxyapatite-coated stainless steel implants. *Journal of Materials Science Letters*, 16, 1964-1966.

Stea, S., Visentin, M., Granchi, D., Cenni, E., Ciapetti, G., Sudanese, A., & Toni, A. (2000). Apoptosis in peri-implant tissue. *Biomaterials*, 21, 1393-1398.

Stulajterova, R., & Medvecky, L. (2008). Effect of calcium ions on transformation brushite to hydroxyapatite in aqueous solutions. *Colloids and Surfaces A: Physicochemical and Engineering Aspects*, 316, 104-109.

Sul, Y. T., Johansson, C. B., Kang, Y., Jeon, D. G., Kang, Y., Jeong, D. G., & Albrektsson, T. (2002). Bone reaction to oxidized titanium implants with electrochemical anion sulphuric acid and phosphoric acid incorporation. *Clinical Implant Dentistry and Related Research*, 4, 78-87.

Sun, L.M., Berndt, C.C., Gross, K.A., & Kucuk, A. (2001). Material Fundamentals and Clinical Performance of Plasma-Sprayed Hydroxyapatite Coatings: A Review. *Journal of Biomedical Materials Research,* 58, 570.

Takaoka, K., Nakahara, H., Yoshikawa, H., Masuhara, K., Tsuda, T., & Ono, K. (1988). Ectopic bone induction on and in porous hydroxyapatite combined with collagen and bone morphogenic protein. *Clinical Orthopaedics and Related Research*, 234, 250-254.

Tassery, H., Pertot, W. J., Camps, J., Proust, J. P., & Dejoy, J. (1999). Comparison of two implantation sites for testing intraosseous biocompatibility. *Journal of Endodontics*, 25, 615-618.

Termine, J. D., & Lundy D. R. (1973). Hydroxide and carbonate in rat bone mineral and its synthetic analogues. *Calcified Tissue International*, 13:73-82.

Uchida, A., Araki, N., Shinto, Y., Yoshikawa, H., Ono, K., & Kurosaki, E. (1990). The use of hydroxyapatite ceramic in bone tumour surgery. *The Journal of Bone and Joint Surgery*, 72-B, 298-302.

Vidigal, G.M., Aragones, L.C.A., Campos, A., & Groisman, M. (1999). Histomorphometric analysis of hydroxyapatite-coated and uncoated titanium dental implants in rabbit cortical bone. *Implant Dentistry*, 8, 295-302.

Viorel, M.R., Chuen-How, N., Max, W., Brigitte, T., Peter, F., & Martin, G.P. (2005). Size-controlled hydroxyapatite naoparticles as self-organized organic-inorganic composite materials. *Biomaterials*, 26, 5414-5426.

Viorney, C., Guenther, H.L., Aronsson, B.O., Pechy, P., Descouts, P., & Gratzel, M. (2002). Osteoblast culture on polished titanium disks modified with phosphonic acids. *Journal of Biomedical Materials Research*, 62, 149-155.

Von Knoch, M., Engh, C. A., Sychterz, C. J., Engh, C. A., & Willert, H. G. (2000). Migration of polyethylene wear debris in one type of uncemented femoral component with circumferential porous coating. *Journal of Arthroplasty*, 15, 72-78.

Wang, F., Wu, X.Q., Sheng, C., Xu, X.Y., Wu, X.H, & Zhang, Z.R. (2003). Effect of ethyl alcohol on calcium phosphate coating by electrodeposition. *Journal of Shanghai Normal University (Nature Science)*, 32(2), 52-56.

Wang, Y., Khor, K. A., & Cheang, P. (1998). Thermal Spraying of Functional1y Graded Calcium Phosphate Coatings for Biomedical Implants. *Journal of Thermal Spray Technology*, 50-57.

Wang, B.C., Chang, E., & Lee, T.M. (1995). Changes in phases and crystallinity of plasma-sprayed hydroxyapatite coatings under heat treatment: a quantitative study. *Journal of Biomedical Materials Research,* 28, 1483-1492.

Wanga, S., Shih, W., Li, W., Hon, M. & Wang, M. (2005). Morphology of calcium phosphate coatings deposited on a Ti–6Al–4V substrate by an electrolytic method under 80 Torr. *Journal of the European Ceramic Society*, 25(14), 3287-3292.

Whitehead, R., Lacefield, W., & Lucas, L. (1993). Structure and integrity of a plasma sprayed hydroxylapatite coating on titanium. *Journal of Biomedical Materials Research*, 27, 1501-1507.

William, A. (1999). The physico-chemical conditions for the precipitation of phosphate with calcium. *Environmental Technology*, 20, 727-733.

Yamashita, K., Yagi, T., & Umegaki, T. (1996). Bonelike coatings onto ceramics by reactive magnetron sputtering. *Journal of the American Ceramic Society*, 79, 3313-3316.

Yong, H., Kewei, X., Jian, L., & Zhu, W. (1999). The structural characteristics and mechanical behaviors of nonstoichiometric apatite coatings sintered in air atmosphere. *Journal of Biomedical Materials Research*, 45(3), 198-203.

Yong, H., Tao, F., Jian, L., & Kewei, X. (2001). Characterization and stability of hydroxyapatite coatings prepared by an electrodeposition and alkaline-treatment process. *Journal of Biomedical Materials Research*, 54(1), 96-101.

Yurong, C., Yukan, L., Weiqi, Y., Qinghong, H., Jinhui, T., Ming, Z., Zhongli, S., & Ruikang, T. (2007). Role of hydroxyapatite nanoparticle size in bone cell Proliferation. *Journal of Materials Chemistry*, 17, 3780.

Zhang, J.M., Lin, C.J., Fend, Z.D., & Tian, Z.W. (1998). Mechanistic studies of electrodeposition for bioceramic coatings of calcium phosphates by an in situ pH-microsensor technique. *Journal of Electroanalytical Chemistry*, 452, 235-240.

Zhang, Y., Tao, J., Pang, Y., Wang, W., & Wang, T. (2006). Electrochemical deposition of hydroxyapatite coatings on titanium. *Transactions of Nonferrous Metals Society of China*, 16(3), 663.

Zhao, Z.W., Li, H.*G.,* Sun*,* P.M., Li, Y.J, Huo, *G.*S., Masazumi, O., & Ryoichi, I. (2002). New method for electro-chemical deposition of bioceramic coatings. *Rare Metals and Cemented Carbides*, 30(1), 6-8.